Lorentz Force Actuator and Carbon Fiber Co-winding Design, Construction and Characterization

by

Yi Chen

SUBMITTED TO THE DEPARTMENT OF MECHANICAL ENGINEERING IN PARTIAL FULFILLMENT OF THE REQUIREMENTS FOR THE DEGREE OF

BACHELORS OF SCIENCE IN MECHANICAL ENGINEERING
AT THE
MASSACHUSETTS INSTITUTE OF TECHNOLOGY

May 2008

Signature of Author:_____
Department of Mechanical Engineering
May 5, 2008

Certified by:_____
Ian W. Hunter
Hatsopoulos Professor of Mechanical Engineering
Thesis Supervisor

Accepted by:_____
John H. Lienhard V
Professor of Mechanical Engineering
Chairman, Undergraduate Thesis Committee

Lorentz Force Actuator and Carbon Fiber Co-winding Design, Construction and Characterization

by

Yi Chen

Submitted to the Department of Mechanical Engineering
on May 9, 2008 in partial fulfillment of the
Requirements for the Degree of Bachelor of Science in
Mechanical Engineering

ABSTRACT

Carbon fiber composites are materials that present many benefits to engineering applications, ranging from aerospace to medicine. This thesis provides background on carbon fiber properties and manufacturing techniques, and outlines the methodology for manufacturing a co-wound carbon fiber and copper coil for use in linear Lorentz force actuators. A conventionally-wound, plastic-bobbin actuator coil and the new, co-wound coil were then tested to compare their electrical, thermal, and mechanical performance. In a needle-free injection application, the co-wound coil demonstrated improved performance over the conventional coil configuration. The carbon fiber coil is lighter by 3.75 ± 0.155 grams, increases the transient heat transfer by 15.7 %, is 2.18 ± 0.13 times stiffer, and can survive a higher compressive force than the conventional plastic bobbin.

Thesis Supervisor: Ian W. Hunter
Title: Hatsopoulos Professor of Mechanical Engineering

Acknowledgments

I would like to thank Professor Ian Hunter and the members of the Bioinstrumentation Laboratory at MIT. In particular, I would like to thank Professor Hunter for serving as my Undergraduate Research Opportunities Program (UROP) advisor and as my undergraduate thesis advisor. I would like to thank him for his inspiration, motivation, support and advice throughout this project. In addition, I would also like to thank Bryan Ruddy for his help in the lab and for helping me revise my thesis. I would also like to thank Dr. Cathy Hogan for her support and for reading through and advising on my research. Ms. Kate Melvin, thank you so much for helping me obtain instruments and for your support.

Thanks to Mr. Pierce Hayward for helping me set up the instrument, obtain data for the stress strain data and for helping me debug the system. To Priam Pillai, Miguel Saez, Bryan Ruddy, Brian Hemond and Chris Bae and other members of the Bioinstrumentation Laboratory, I had a great time working with you throughout the year. Thanks for all your practical advice and encouragement about my thesis as well as about graduate school. I wish you the best in your research!

I would also like to thank my Father, Mother and Sister for their support throughout the process. Thank you for believing in me.

Contents

Introduction 11
1. Background 13
1.1 Carbon Fiber Technology 13
1.1.1 Microstructure 13
1.1.2 Carbon Fiber Properties 15
1.1.3 Carbon Fiber Polymer Composite Properties and Manufacturing 16
1.2 Lorentz Force Technology 20
1.2.1 Applications 20
1.2.2 Theory of Operation 21
1.3 NFI Technology 22
1.3.1 NFI History 22
1.3.2 Lorentz Force NFI Device Development 25
2. Design and Modeling 27
2.1 Carbon Fiber and Copper Materials 27
2.2 Carbon Fiber Bobbin 28
2.3 Carbon Fiber Co-winding 30
3. Manufacturing 32
3.1 Coil Winding Setup 32
3.2 Bobbin Manufacturing 33
3.3 Co-winding Manufacturing 36
4. Characterization 40
4.1 Impedance Analysis 40
4.4 Heat Transfer Analysis 41
4.3 Dynamic Mechanical Analysis and Compression Strength 44
5. Results and Discussion 46
5.1 Impedance Analysis 46
5.2 Temperature Analysis 49
5.2.1 Comparison of Free-Air and In-Casing Temperatures 49
5.2.2 Free-Air Model 51
5.3 Dynamic Mechanical Analysis 59
5.4 Compression Strength 61
6. Conclusions and Recommendations 64
References 66
Appendix 68

Table of Figures

Figure 1: SEM photograph of pitch-based Thornel P-100 carbon fiber 14
Figure 2: Carbon fiber tubing 17
Figure 3: Nose part of a Boeing 787 Dreamliner 18
Figure 4: S-N curve showing fatigue behavior of composite materials 19
Figure 5: Magnetic field configuration for current NFI 21
Figure 6: The CrossJect Controlled Reaction NFI Device 23
Figure 7: Glide SDI and PowderJect. 24
Figure 8: Lorentz Force NFI Device Design Iterations. 25
Figure 9: Competitive Landscape for NFI devices. 26
Figure 10: Carbon Fiber Bobbin Design. 29
Figure 11: Coil deformation at 50 N and 2 Hz in compression 30
Figure 12: Carbon fiber co-winding structure. 31
Figure 13: Iteration one and two of coil winding setup 33
Figure 14: Materials used for the manufacturing of carbon fiber bobbins 34
Figure 15: Comparison of carbon fiber and plastic bobbin. 35
Figure 16: Mandrel setup and coil in the process of being wound. 37
Figure 17: High temperature vacuum oven used to cure carbon fiber assemblies. 38
Figure 18: Finished carbon fiber and copper co-wound Lorentz force coil 38
Figure 19: Instrumentation for Impedance Analysis 41
Figure 20: Instrumentation for temperature analysis. 42
Figure 21: LabVIEW program for Temperature Analysis. 43
Figure 22: The instrumentation for dynamic mechanical testing and static mechanical testing. 44
Figure 23: Dynamic mechanical analysis and compression strength analysis LabVIEW VI. 45
Figure 24: Gain and Phase information for three different types of coils. 46
Figure 25: Gain and phase as a function of the vertical position of the co-wound coil. 48
Figure 26: Temperature profiles of the original polysulfone and the co-wound coil. 50
Figure 27: Original plastic bobbin based coil temperature and heat simulations 55
Figure 28: Co-wound coil temperature and heat simulations 57
Figure 29: Force and displacement in an isotonic test on a carbon fiber bobbin. 59
Figure 30: The displacement vs. force to show viscoelastic behavior and hysteresis 60
Figure 32: A crushed coil between the platens. 62
Figure 33: Crushed coils showing different failure modes. 62
Figure 34: Force as a function of displacement for compressive strength testing 63

Introduction

Lorentz force actuators are a common type of linear actuator used in many applications, from speakers to vibration and materials testing equipment. The current practice in manufacturing coils for Lorentz force actuators is to wind thin copper wires around an aluminum bobbin. In order to increase performance, some voice coils are wound on bobbins made of titanium or phenol resin-coated glass cloth [1]. Bobbin-based Lorentz force coil assemblies have many advantages and may be adequate for certain applications. However, there are a few high bandwidth, high force and thermally limited applications which would benefit from a more advanced design. This thesis introduces another method for creating Lorentz force coil assemblies by co-winding the copper with carbon fiber. In addition to increases in strength for the overall assembly, mass can be reduced, eddy currents can be minimized and the thermal properties of the coil can be improved.

Carbon fiber reinforced plastics are becoming more common today in everything from commercial airplanes to mountain bikes. The material is made from strands of carbon fiber cloth coated with special resin. The composite material has anisotropic properties depending on the direction of the fibers. Carbon fiber can be co-wound with copper coils to create a new composite material with special properties which can be derived from the strength in the carbon fiber, the thermal and electrical properties of copper.

One specific application which can benefit from this copper-carbon composite is the Lorentz force coil for a needle-free injection (NFI) device. Needle free injection is a process whereby a jet of fluid passes through a small orifice at high speed and pierces the skin to deliver a liquid or powdered drug. This concept avoids some of the sharps hazards as well as training and patient compliance difficulty of needles and could eventually replace needle injections in the future [2]. However, there are many practical issues that have made mass implementation of NFI difficult such as contamination concerns. An NFI device under development at the MIT Bioinstrumentation laboratory has attempted to solve some of the practical difficulties in NFI technology [3]. This device uses a Lorentz force actuator to create jets of fluid. This particular actuator has performance and size constraints that require better coil construction. These

constraints include high bandwidth, forces on the order of 200 N, power dissipation on the order of 2 kW, and compact physical size. Future applications for the NFI device include injection of powder medications at high speeds, which may require the Lorentz force actuator to create even higher forces.

This paper proposes a method for constructing carbon fiber and copper co-wound Lorentz force coils as well as models for predicting its performance. The resulting coils are also compared with the current NFI coils in the performance parameters of limit load, dynamic mechanical response, electrical impedance and heat dissipation. The models are also verified based on test data.

1. Background

In order to design a carbon fiber and copper co-wound structure, the properties of the carbon fiber material and the requirements of the Lorentz force actuator must first be understood. Carbon fiber properties, manufacturing processes, current research and modeling techniques are first explored. Then, the requirements of Lorentz force actuators in general as well as the specific requirements of the NFI device are also discussed.

1.1 Carbon Fiber Technology

Fiber reinforced plastics are a strong and light composite material that is composed of a strong fibrous material interspersed with plastics such as resins or epoxies. In some cases, the composite is reinforced with Kevlar, aluminum, fiberglass and even carbon nanotubes [3]. The strongest and most versatile fiber reinforced plastics employ macroscopic carbon reinforcement fibers, and are thus called carbon fiber reinforced plastics (CFRPs). Initially, the expensive manufacturing process restricted use of the material to high end products for aerospace, sailboats, and performance racing vehicles. However, as manufacturing techniques have improved, CFRPs have found their way into sporting equipment and other consumer goods. In order to understand the material, the carbon fiber microstructure, properties, and manufacturing techniques are discussed.

1.1.1 Microstructure

Carbon fibers can have microstructures ranging from crystalline to amorphous, depending on the manufacturing procedures. The crystalline type has carbon atoms that are arranged in a two-dimensional honeycomb structure, similar to the form of graphite. Carbon atoms inside a layer are bonded by delocalized covalent bonds. Bonding between layers is based on Van der Waals forces, so the layers can easily slide past each other. This crystalline structure allows carbon fiber to have high electrical and thermal conductivity in the plane parallel to the layers but have good thermal and electrical insulation in the plane perpendicular to the layers. In addition, the layers are perpendicular to the fiber axis due to the preferred crystal orientation, giving carbon fiber its high elastic modulus. In amorphous carbon fibers, there are carbon layers but the layers are not

parallel to each other [5]. In Figure 1, the distinct layers that comprise a single carbon fiber can be seen. The orientation of the layers is called the texture.

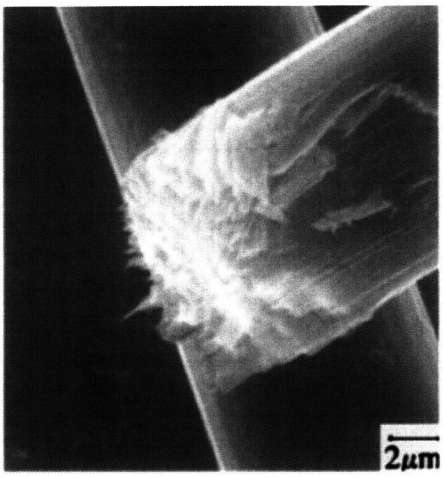

Figure 1: SEM photograph of pitch-based Thornel P-100 carbon fiber showing the orientation of layers inside a single carbon fiber. Reproduced from [5].

There are two main methods for manufacturing carbon fibers. Commercial fibers can be created from pitch or polyacrylonitirile (PAN). Pitch is processed through melt spinning and infusiblized to convert the material into its flameproof and stable form. PAN precursors are wet spun and stabilized in an oxidizing atmosphere. General purpose and high performance fibers are then carbonized and graphitized at temperatures above 2500 °C. Higher graphitization temperatures result in better orientation. Since pitch is more graphitizable than PAN, pitch-based carbon fibers can achieve a higher elastic modulus (up to 80 % of the theoretical modulus of a single graphite crystal). PAN-based fibers can achieve a higher tensile strength and elongation, mainly because shear is easier between carbon layers in a graphitized pitch fiber [5].

Using these manufacturing techniques, here are three main categories of carbon fibers including general purpose, high performance and activated carbon fibers. General purpose carbon fibers are amorphous with low tensile strength ad tensile modulus. Activated carbon fibers have a large number of small pores which can be used as adsorption sites. There are two main types of high performance carbon fibers — high strength and high modulus. The high strength carbon fibers are classified as those with strength greater than 3 GPa and a breakage strain between 1.5 and 2 %. The high modulus types are classified as fibers with elastic modulus greater than 300 GPa

and a breakage strain below 1 %. The tensile stress-strain curves for fibers are generally straight lines up to fracture such that the ductility for fibers is very low [6].

1.1.2 Carbon Fiber Properties

The microstructure of carbon fiber contributes greatly to some of its attractive properties, including low density, high tensile strength, high thermal conductivity, low thermal expansion coefficient and high creep resistance. Carbon fiber also has some unfavorable (for the copper co-winding application) characteristics such as low electrical resistivity, anisotropy, low strain to failure, and low compressive strength compared to tensile strength. Each of these properties can be exploited or compensated for to design the best composite for our application.

Carbon fiber has a tensile strength that is an order of magnitude higher than that of steel and a density one-fifth that of steel, making it a strong and light substitute. On the other hand, compressive strength can be anywhere from 12.5 to 58.9 % of the tensile strength (0.54 to 2.06 GPa) depending on the manufacturing technique used to create the fiber. These values are still comparable to steel but are sufficiently different from the tensile strength that structures under compressive loads require [7]. Pitch-based carbon fibers have lower compressive strength and compressive failure strain than PAN-based fibers due to the greater orientation of carbon layers in pitch-based fibers. Pitch fibers break in compression when the carbon layers shear with fracture surfaces at 45 degrees to the fiber axis. PAN fibers instead typically buckle in compression [5].

Low electrical resistivity could also cause potential problems for co-winding. When Lorentz force coils pass through a magnetic field, any conductive material that forms a closed loop inside the magnetic field will carry an induced current, and these eddy currents tend to damp the motion of the coil. The resistivity decreases with temperature increases, potentially exacerbating eddy current losses when increased losses are most problematic. This particular phenomenon can be reduced by selectively orienting the fibers or arranging fibers to eliminate closed loops.

Certain carbon fibers have thermal conductivities higher than that of copper (P-100, P-120 and K110X) with thermal expansion coefficients that are lower (some of which are even negative). For example, K110X has a thermal conductivity of 1100 W/mK and a coefficient of thermal

expansion of about -1.6×10^{-6}. Most carbon fibers on the market today, however, have thermal conductivities that are below that of copper, in the range of 10 W/mK [5].

1.1.3 Carbon Fiber Polymer Composite Properties and Manufacturing

Carbon fiber composites have many advantages because the carbon fibers can be used as reinforcements into other materials. Some of the more common types of composites include polymer matrix composites, metal matrix composites, carbon matrix composites and ceramic matrix composites. The first know polymer composite was used in the 1930s for manufacturing a boat hull with fiberglass and a polyester fabric laid on a foam mold [8].

Polymer composites are by far the most common because of low processing temperatures and ease of fabrication [5]. The two types of polymer matrix composites are thermoset and thermoplast processes. Theroplasts involve bonding plastics to carbon fibers and have the advantages of high toughness, high environmental tolerance, thermal shaping, weldability, preprocessing possibilities, no curing, and unlimited shelf-life. However thermosets such as epoxies have more flexibility in processing methods, lower processing temperatures, lower viscosities (allowing better wetting) and better surface treatments. Because of these characteristics, thermosets are more common [5] and are more optimal for copper co-winding.

Today, five of the most common manufacturing processes in thermoset polymer composites include wet lay-up, dry lay-up, resin induction, compression molding and filament winding. Depending on the desired surface finish, geometry, production quantities and strength requirements one of these methods may be selected. Other methods for production including protrusion also exist for producing rods, tubes and sheets of CFRPs in a continuous fashion.

Wet lay-up is generally used to create surfaces or shells of CFRP. First, a mold shape is created, polished, waxed and covered with releasing agents. Then a two-part epoxy is mixed and applied to the oriented carbon fiber fabric. This "wet" fabric is then placed onto the mold and formed into the desired shape. Release fabric with pinholes may be placed on top of the carbon fiber material to create a surface finish on the material. Depending on the application, the mold may

be further constrained to create pressure on the epoxy inside the mold and the assembly may be placed in a vacuum-sealed bag or autoclaved to remove air bubbles. The removal of bubbles may be important if the application requires high strength because the bubbles may create critical stress areas inside the CFRP. The epoxy is then cured at temperatures in the range of 40 °C to 200 °C and may take eight hours or more. After the curing, the release cloth and molds are removed and the CFRP is trimmed and finished [5].

Dry lay-up differs from wet lay-up in that the epoxy is pre-impregnated into the carbon fiber fabric and the material is applied to the mold like an adhesive film. The dry lay-up method uses the least amount of resin and will tend to be lighter than wet lay-up products. These prepreg parts generally have fewer bubbles or pinholes than wet lay-up techniques but in order to eliminate pinholes completely, these parts must be cured at autoclave pressures. Figure 2 shows a standard carbon fiber tube made from bi-directional woven sheet.

Figure 2: Carbon fiber tubing. This configuration is generally created from dry lay-up or resin induction. Reproduced from [9].

Resin induction is another useful method in which a dry fabric and mold are first assembled and placed in a bag. A vacuum is created inside the bag which pulls the resin from a tube at one end of the assembly to another thereby evenly distributing the resin. This method results in good surface finishes and can help distribute more viscous resins throughout a part [8].

Compression molding is a fast and relatively clean method for handling carbon fiber assemblies. A two-piece male and female mold, often made of fiberglass or aluminum, is created in which the carbon fiber and resin are placed. The assembly can be bolted and easily moved and stored without a vacuum. The disadvantage to this method is that it uses more mold material than other methods.

Lastly, filament winding may be desirable for complex shapes. Filament winding involves winding strands of carbon fiber (from rovings) around a male mold or mandrel that is rotated. A carriage containing a fiber tensioner lays down the fibers at a desired tension, pitch and thickness. Lower tension results in a more flexible structure while higher tension results in a more rigid structure. Orientation at a high angle produces parts with better crushing strength while a tighter coil provides better tensile strength. Each layer can be controlled or plied into different orientations to provide strength in different directions. Figure 3 on the left shows a Boeing 787 Dreamliner nose section that is composed of a single composite part.

Figure 3: Nose part of a Boeing 787 Dreamliner composed of a single composite part before doors and windows have been cut. Reproduced from [10].

The resin may be applied before the fiber reaches the winding, pre-impregnated after the winding is complete or post-impregnated. The assembly is then covered with release cloth and cured. Afterwards, the mold or mandrel can be removed leaving the hollow part. This method is commonly used to create golf clubs, oars, pressure vessels aircraft fuselages and even missile casings [5]. Complex geometries can be designed today using pattern generation software such as FiberGrafiX™ and CADWIND™ [7].

Polymer composites have many additional desirable properties such as low densities, higher stiffness than titanium, good fatigue resistance, a low friction coefficient, corrosion resistance, structural vibration damping and a high thermal conductivity [5]. Figure 4 shows the S-N curve and the fatigue behavior of many composite materials including carbon fiber.

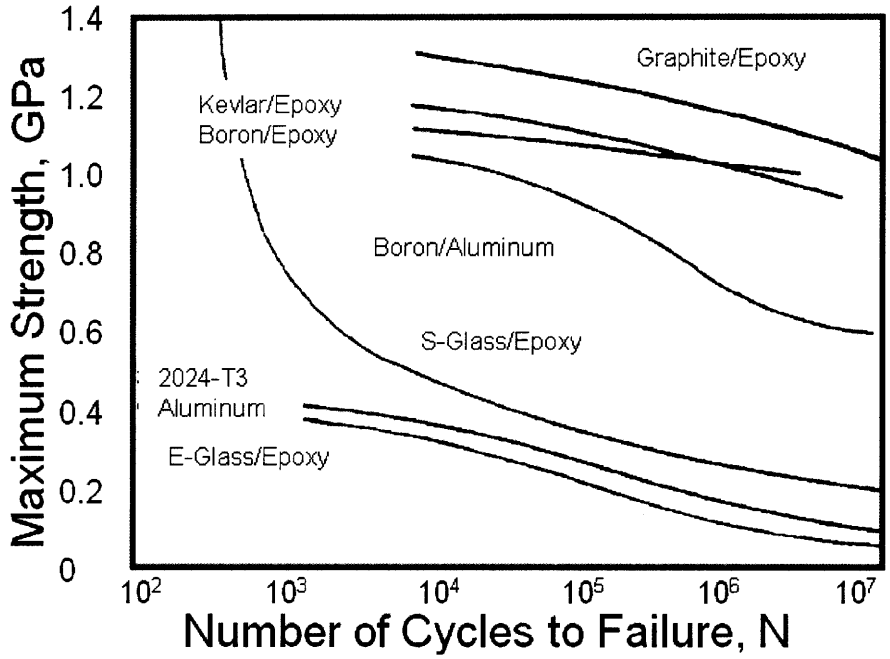

Figure 4: S-N curve showing fatigue behavior of composite materials and aluminum. Unlike aluminum which may fail. Reproduced from [11]

One particularly desirable property is the fatigue behavior of carbon fiber composites. Even at extremely high maximum stress levels, carbon fibers have a virtually unlimited lifespan under fatigue which is perfect for applications where the product may be subjected to high forces regularly. Because its performance is better than aluminum, CFRPs are an ideal candidate for coil assemblies for linear Lorentz force actuators.

1.2 Lorentz Force Technology

1.2.1 Applications

The most common applications of the Lorentz force is in voice coils as well as vibration and materials testing equipment. Each of these applications has an optimized configuration to handle different amounts of force and operate at different bandwidths. Lorentz force actuators have gained popularity in industries where precision position control is required. One such application is to use Lorentz force coils to control the angle in beam steering mirrors [12]. Additional applications include actuation for biomimetic robotics including robotic fish fins and robotic bird wings.

For high performance subwoofers, the frequency response is in the range of 18 to 2000 kHz for a 2 Ω coil with 0.0762 m diameter and 6 layers of coil. These voice coils often have maximum power ratings in the range of 8 kW. Because of the frequency response needed by these coils, they are generally made to be lightweight which may make them fragile. Most bobbins are made with aluminum housings which cause eddy currents to flow through the bobbin damping the motion of the coil at higher frequencies. In order to handle these large forces and frequencies, high performance voice coils often have features such as pure titanium bobbins and coil wires that are coated in ceramics [1].

The power handling capabilities of a coil are limited by its heat generation (due to ohmic heating) and its heat dissipation capabilities. The housing for many coils provides heat sinking abilities preventing the coil from heating too quickly. In addition, a moving coil can provide convective cooling. The worst case scenario is when the coil is outside the housing exposed to the air where natural convection is ineffective in removing adequate amounts of heat. Some coils are built from special materials which allow them to be placed in ferrofluids to provide cooling when subjected to higher power conditions. However, this causes manufacturing difficulties, increases mass and may also damp the motion of the coil.

1.2.2 Theory of Operation

The Lorentz force is a force on a point charge caused by an electromagnetic field. The force on the particle is proportional to the field strength B and the current I that is perpendicular to the field multiplied by the number N of conductors in series each with length L. When a current is applied to the coil, it creates a magnetic field which interacts with the magnetic field from the permanent magnet using the cross product,

$$F = ILN \times B \quad . \tag{1.2.1}$$

There are two main types of voice coil configurations known as the overhung and the underhung configurations. In the overhung configuration, the coil windings are taller than the height of the magnetic field gap. This configuration has the advantage of higher sensitivity but suffers from higher coil mass. The underhung configuration is when the coil windings are shorter than the height of the magnetic field gap. This configuration has the advantage of lower mass but creates a bigger control problem if the coil leaves the gap.

For the overhung configuration shown in Figure 5, the magnetic field only interacts with the current-carrying wires at a single region near the top plate where the field lines are perpendicular to the direction of the current.

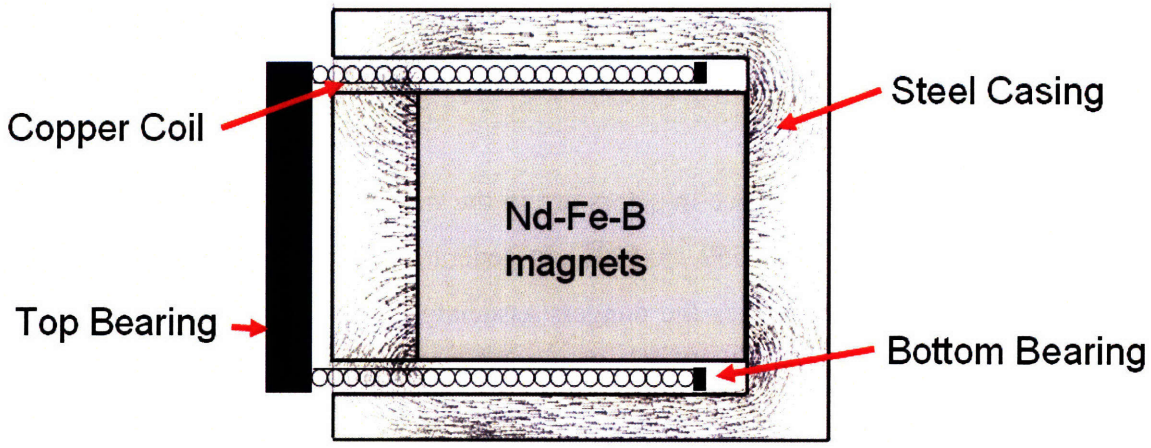

Figure 5: Magnetic field configuration for current NFI. The magnetic field crosses the coil at the top plate where a force is then generated. Reproduced from [13].

If the current is coming out of the page at the top of the drawing and going into the page at the bottom of the drawing, the force generated would cause the coil to move to the left relative to the casing. If the current was reversed, then the direction of the force would also be reversed. Since the current goes as the square root of the power consumption, there are only a few ways in which to improve the force output of the voice coil if the gap geometry is to remain the same. First, the magnetic field strength can be improved, secondly the power input into the coil can be increased, and lastly, the number of windings N that enters the magnetic field can also be increased. For a fixed geometry, a force constant K can be defined as LNB which indicates how much force the coil can output for an increase in the current.

1.3 NFI Technology

1.3.1 NFI History

Needle free injection was first proposed by A. Beclard in 1866. A simple needle free injection device was first patented in 1943. The original concept was that fluids at high velocities could penetrate skin rendering the needle injections obsolete [2]. Needle free injectors alleviate many of the practical issues associated with needles including complex injection techniques, disposal costs, cross contamination risk, aichmophobia (fear of needles), and pain on the site of injection. First, health care professionals must be specially trained to aspirate, find the correct depth of injection, keep the needles steady and avoid being hurt with the used needle. Needle free injection, on the other hand, requires little training which allows it to be easily utilized at home by the patient [14].

The orifice sizes of most needle free injectors are in the range of 76 to 360 μm while the most common diameter for a needle is 559 μm [14]. In general, needle free injection is less painful, reduces needle injuries, and reduces the dangers associated with sharps disposal. In addition, injections by needles also create a sphere of medicine around the area of the injection while needle free injection shows dispersion in the desired layer of the skin which improves the immune response [15].

Despite the fact that the technology has been available for over 60 years, Needle free injection has not become widespread because of concerns of contamination, variation in the fluid jet, drugs pooling on the skin, volume restrictions, incomplete deliveries, and localized bruising and bleeding. One particular device, the Ped-O-Jet, was widely used in the 1970s and 80s but was known to slice tissue if not held tightly to the skin [3]. Today, there are a few needle free personal injection products which utilize small pressure capsules or tunable springs which implement this concept.

Spring powered devices are commonly used for diabetic patients. These devices are light weight from 77 to 172 g each. A tunable spring may used to control the injection for different people. However, the tuning process involves trial and error and is not suitable for mass immunizations. Gas powered injectors can create rapid sequential injections which is ideal for mass immunizations, military use, or humanitarian efforts. These devices generate greater forces which allow more of the drug to be delivered. However this concept also suffers from controllability issues, gas leakages, costs of replacing the gas supply, and noise generation from the release of the gas [14]. Figure 6 shows the CrossJect which uses another method to create the injection force. It utilizes a controlled chemical reaction to create gases at high pressures. The CrossJect system eliminates the gas leakage and gas supply issues associated with some NFI devices. However, it has the same controllability and tuning issues as spring loaded devices.

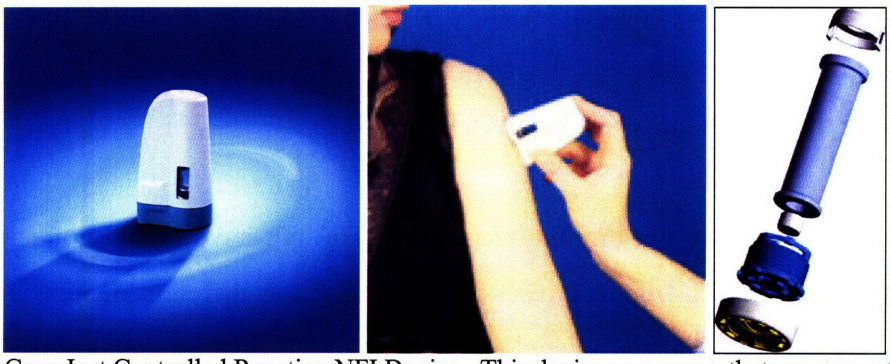

Figure 6: The CrossJect Controlled Reaction NFI Device. This device uses gases that are generated at the same time as the injection and allows some ability to tune the injection profile. The image shows the dimensions of the CrossJect (left), the use of the device (middle), and the sub assembly including the glass tube, piston, and nozzle (right). Reproduced from [16].

There is another class of needle free injectors able to inject powders at high velocities. Large quantities of vaccines are ruined each year due to delays in transport, ineffective handling, and equipment failures. One solution to this problem is to use a powdered form of the vaccine, such as in Epidermal Powder Immunization, which removes the hazards of the cold chain. This approach, on the other hand, introduces the difficulty of injecting micro-particles into the skin. Nominal velocities on the order of 420 to 640 m/s are needed for the injection of high density micro-particles with diameters of 1.78 to 3.03 μm into human skin [17]. Lower velocities on the order of 260 m/s are needed for larger particles with diameters of 20 to 40 μm in size [18]. Figure 7 shows the two most common products on the market today which are capable of delivering solid drugs including the Glide SDI and PowderJect.

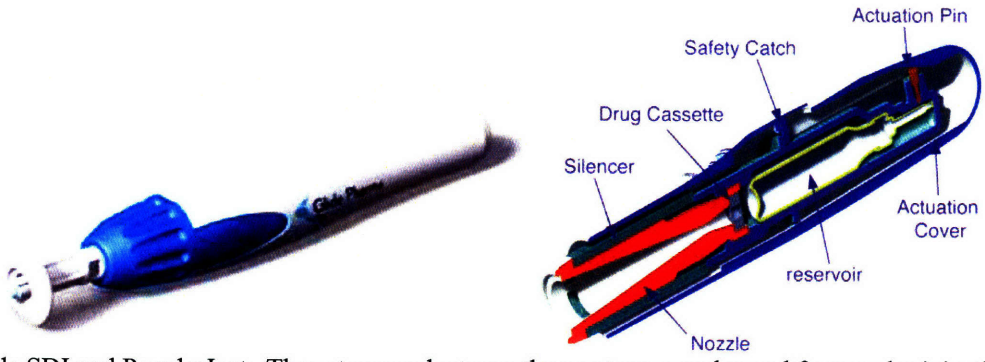

Figure 7: Glide SDI and PowderJect. These two products are the most commonly used for powder injections. The Glide SDI pushes the solid powder into the skin directly at high speeds (left, reproduced from [19]) while the PowderJect system utilized high pressure gases to actuate powders (right, reproduced from [20]).

The PowderJect device is the most commonly used of the two. It uses a helium storage tank at pressures in the tens of atmospheres. A small drug cassette is located between two membranes which burst when the gas is released. A show wave propagates down the nozzle causing the particles to entrain with the gas. As the gas hits the surface of the skin, it deflects while the particles puncture the skin due to their larger inertia [20].

Products on the market today are limited because they do not have tunable injection profiles to accommodate injection into different types of skin injection to different depths. An NFI device based on Lorentz force coils is being developed at the MIT Bioinstrumentation Laboratory. The current that is applied to the coil is tunable allowing different injection profiles to be created with the same device. Feedback control could also be used to dynamically alter the injection profile to achieve the desired result [21].

1.3.2 Lorentz Force NFI Device Development

Since 2004, a Lorentz force actuator NFI device has been in development at the MIT Bioinstrumentation laboratory. The original device was large and used a BEI Kimco Magnetics LA25-42-000A motor [21] [22]. Later, smaller coils were wound to produce smaller handheld devices which would be easier to handle for mass market applications and for lab applications [13] [15] [23].

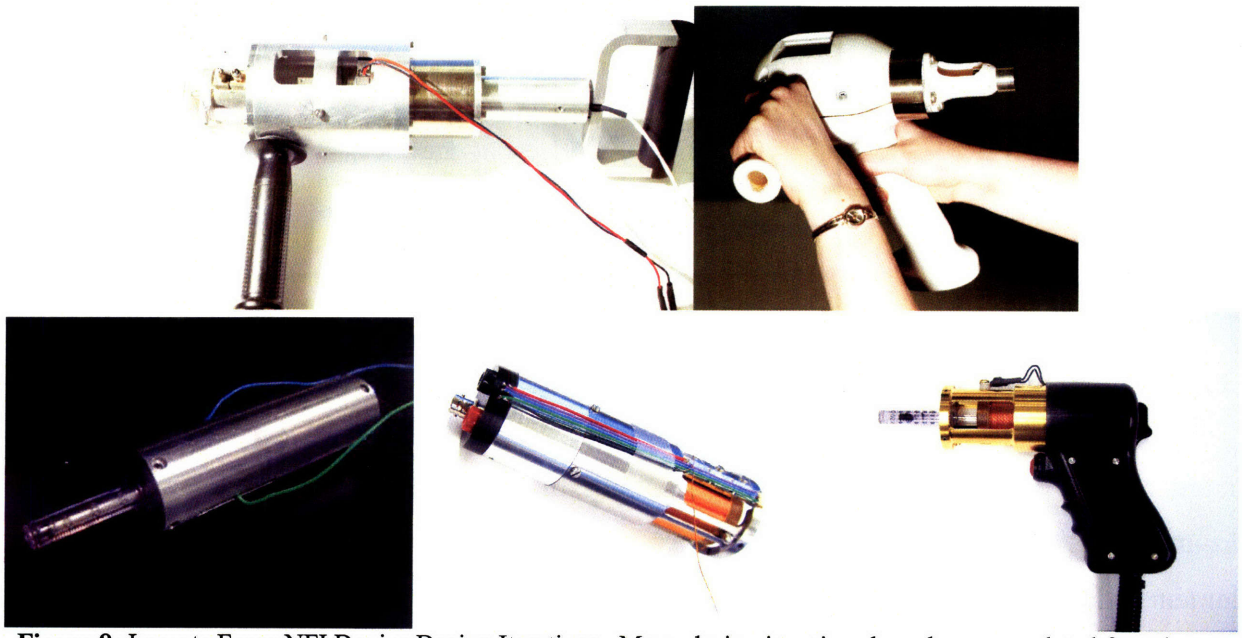

Figure 8: Lorentz Force NFI Device Design Iterations. Many design iterations have been completed from larger research versions (top left and top right, reproduced from [22]) to smaller hand held versions (bottom left, reproduced from [13]). The most recent version is used in both robotic fin actuation and for laboratory research (bottom middle and left, reproduced from [15]).

The current Lorentz Force NFI device is a handheld gun which can create an instantaneous force in excess of 200 N and inject liquid quantities of up to 250 μL at maximum fluid speeds of 235 m/s [23]. The coil assembly is currently approximately 50 g with an inner coil diameter of 26 mm and an outer diameter of 32 mm. The height of the assembly with the top plate is 47 mm while the coil only occupies 38 mm. The stroke of the most current version used for laboratory experiments is 30 mm with a force constant of 10.8 ± 0.5 N/A. The Neodymium Steel Boron magnets with a field strength of 397.9 kJ/m^3 are used to create a magnetic field in the gap of approximately 0.6 T [3]. In this framework, a carbon fiber co-wound coil is being developed to increase the force delivery and power handling capabilities of the NFI device.

The competitive marketplace for needle free injection devices can be broken up into devices which inject solids and devices which inject liquids. In addition, there is a drive to produce smaller, lighter weight and low cost devices for mass distribution. Figure 9 shows the competitive landscape for NFI devices that are currently on the market.

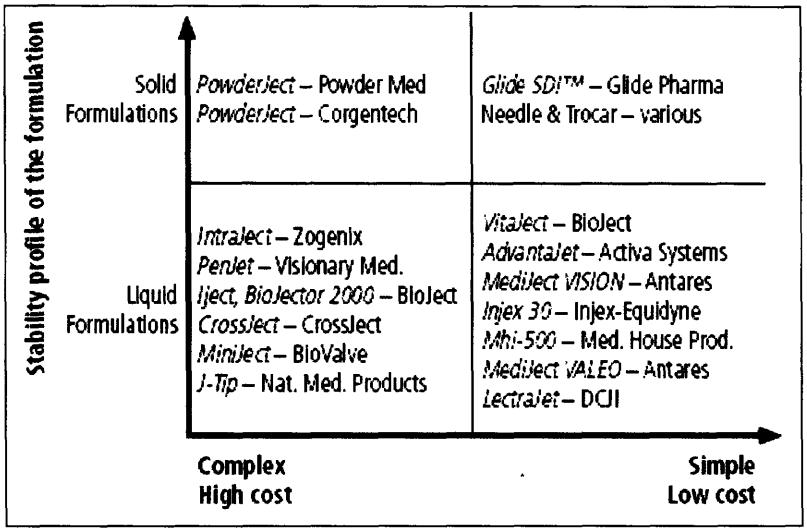

Figure 9: Competitive Landscape for NFI devices. In order to be competitive, an NFI device needs to be simple, low cost, light weight, and flexible. Reproduced from [19].

In order to one day cross into the solid formulations, the NFI device must be capable of higher driving forces which implies that the coil must be able to higher power both in the thermal domain and the stress strain domain.

2. Design and Modeling

In designing a carbon fiber and copper co-wound coil, the design goals are to:

- Increase the dynamic stiffness of the assembly
- Increase the maximum force capability (strength)
- Increase thermal handling capabilities (heat dissipation)
- Maintain the ability to operate at temperatures above 200 °C
- Minimize eddy current losses
- Create a stronger and lighter coil for better dynamic performance

One approach is to create the coil with composite material such as carbon fiber where the strength, temperature capabilities, conductivity and other properties can be individually selected and optimized.

2.1 Carbon Fiber and Copper Materials

In order to achieve some of the design goals, the materials must be carefully selected. The magnet wire used to create the actuation force must have a high temperature coating and 28 gauge heavy (double coated) wires which conform to the MW-35C standard were selected. It has a polyester basecoat and a polyamide-imide topcoat which has a minimum temperature handling capability of 200 °C. The topcoat is capable of bonding to itself if heated to above 230 °C [24].

The resin must also be carefully selected to handle high temperatures and stresses. Most high temperature epoxies have extremely high viscosities making it more difficult to wet the carbon fibers. Laminating epoxies produced by Pro-set were selected for the combination of low viscosity and high temperature capabilities [25].

Of the two types of high performance carbon fibers, a high strength carbon fiber was selected. Carbon tows with three thousand and six thousand individual strands per ribbon (3K and 6K respectively) form were obtained with a quoted tensile strength of 3.53 GPa, a tensile modulus of

230.3 GPa. The material has a low density of 1.76 kg/m^3 which makes it ideal for creating a low mass coil [26].

2.2 Carbon Fiber Bobbin

Initially, a bobbin form of carbon fiber was designed to compare the benefits of using carbon fiber instead of using acetyl copolymer or polysulfone. Carbon fiber is an electrically conductive material which may cause eddy currents if a complete winding doubles back on itself within the distance of the top plate (see Figure 5) thereby completing a loop. However, more strength is needed in the vertical direction leading to a bobbin design with vertically oriented carbon fiber strips. Between these strips, the laminating epoxy serves as an electrical insulator which prevents a complete loop from forming. Most carbon fiber applications use both a vertical and a lateral woven pattern to create strength in multiple directions. In this case where eddy currents and mass are a concern, the copper itself can be used as horizontal reinforcement. Carbon tow with 6 thousand fibers in each ribbon was used in the construction in order to achieve a uniform thickness. Each 6K ribbon has a thickness of approximately 182.9 μm.

In order to create a bearing surface, a top and bottom bearing plates were created with the same outer dimensions as the original bobbin. The bottom bearing, which has a thickness of 3 mm, also serves to constrain the coil during winding and provides a surface for forces to collect. Six holes that are each 2 mm were drilled in the top bearing (which has a thickness of 6 mm) to allow air to bleed through the top surface. The middle hole was threaded to allow the attachment of a piston for the injector. A linear guide hole of 4 mm along with two holes for attaching threaded press-fit electrical connectors were also drilled. A slot with a diameter of 1.5 mm was also created to allow the placement of a linear potentiometer which is used to determine the position of the coil. In order to incorporate this top plate with the carbon fiber structure, slots were also cut at the top to insert the vertical carbon fibers to create better contact between the carbon fibers and the top plate.

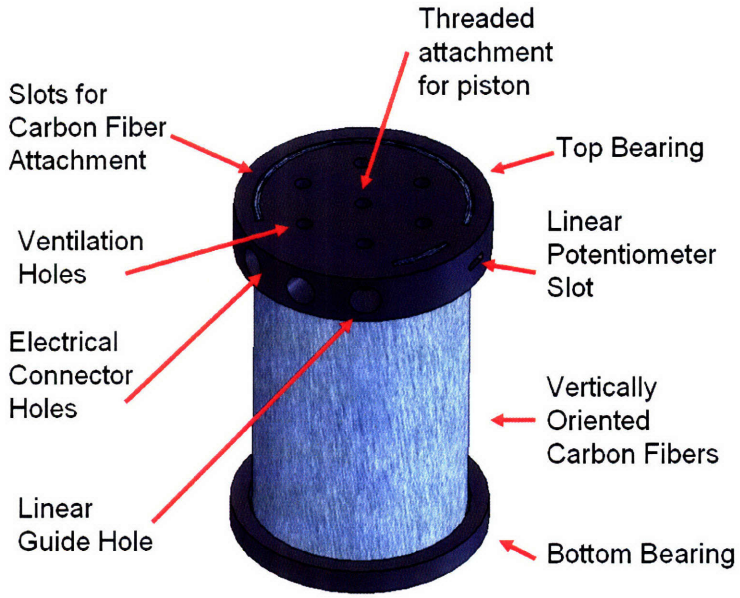

Figure 10: Carbon Fiber Bobbin Design. The design includes the vertically oriented carbon fibers with a top and bottom bearing plates which bear the frictional load of the coil against the walls.

Composite materials are notoriously difficult to machine. Carbon fiber that is filed or drilled will tend to create loose particles which may be inhaled causing a health concerns. Because of the complexity in the geometry of the top plate, carbon fiber is not used to create these shapes. After the bobbin is manufactured, the copper coil can be easily wound onto the carbon fiber tube.

One of the issues with bobbins for Lorentz force coils is the inability to transfer forces from the outer copper layers directly to the primary force surface. The copper wires must either transfer the force through the layers of copper wire above it or through the intermediate wires between it and the bobbin through a shear force. This force transfer may be ineffective due to wire shifting which can occur when the copper windings are not perfectly stacked, when the forces are high enough for the copper and outer coating layers to undergo deformation or when the bobbin deforms. Figure 11 shows one case where the compression on the coil causes a plastic bobbin coil to deform.

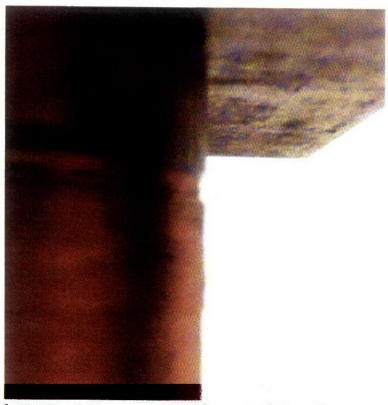

Figure 11: Coil deformation at 50 N and 2 Hz in compression. This view is of the coil is the top corner between two platens. In this failure mode, the coil displaces horizontally causing jamming and ineffective transfer of forces.

The coil in the image was subjected to 50 N at 2 Hz. The force is well within the range of forces coils are subjected to at a frequency that is in the range for coils used in robotic fish fin actuation and well below the speeds at which NFI fires. This failure mode can cause jamming and ineffective force transfer. For these reasons and many others a co-wound structure is preferred.

2.3 Carbon Fiber Co-winding

A vertical structure for the carbon fiber orientation was chosen because it gives the maximum tension and compression strength in the primary force direction. Multiple designs were considered including a version with multiple co-wound layers, different number of carbon fiber strands (1K up to 6K), and different numbers of coils per transition region. Many of these designs were constructed and stress tested. Figure 12 shows the design with an inner and outer co-wound layer.

This design has multiple components including a top bearing, a bottom bearing, thirty-four carbon fiber strands that are each double the coil length, a carbon fiber outer film, and laminating resin. The bobbin still maintains a bottom bearing and a top bearing with electrical and piston connections. The top bearing is used to transfer forces and to provide electrical and piston connections. The bottom bearing serves as a second linear guide and also provides structure for the co-winding process.

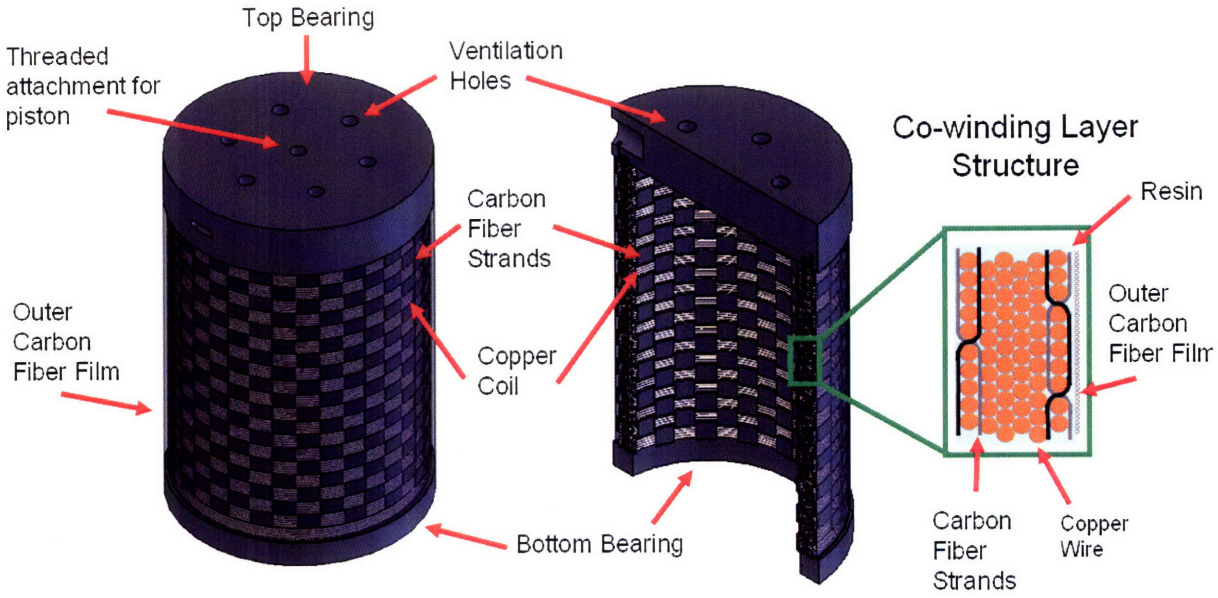

Figure 12: Carbon fiber co-winding structure. The inner and outer layers of coil are wound with alternating layers of carbon fiber strands.

From the inside to the outside of the structure, there is a co-wound inner layer with copper, four layers with no carbon fiber and a last outer layer with carbon fiber. The inner layer is used to transfer forces from the copper upwards, the walls of the carbon fiber are used to constrain a column of five copper wire layers to more effectively align the transfer of forces. The outer layer constrains the outer surface of the wire. The transition regions were two carbon fiber strands cross is the weakest position in terms of buckling. Therefore, the inner and outer co-wound layers have transition regions that alternate in position. Since both sides are rigidly constrained, the center columns are also held in place. In addition, resin is added to all the interstitial spaces to maintain the position of the coils and to facilitate heat transfer.

One of the concerns is that the coil density inside the magnetic field may decrease due to the occurrence of alternating layers. However, the reduction in the density of copper is in the range of 1.9 % since the thickness of 3K fibers is 96.5 μm. Thinner ribbon can be obtained to reduce loss in copper density even more. In addition, there is a translucent carbon fiber film (also known as tissue or veil) with a thickness of 50.8 μm on the outer layer which helps distribute the resin evenly during the manufacturing process.

3. Manufacturing

The manufacturing of co-wound coils includes working with wire tensioners for the copper wire as well as special equipment for laying up and curing carbon fiber composites. In order to co-wind these copper with carbon fiber, a novel manufacturing technique needed to be developed with incorporated wet lay-up, compression molding and filament winding techniques.

3.1 Coil Winding Setup

A coil winding setup was created at the MIT Bioinstrumentation laboratory using a servo-controlled fourth axis on a Dynamite 1007 CNC milling machine. The fourth axis was positioned to rotate on the horizontal axis. In addition, two different coil tensioners obtained from Aumann in Germany were used [27]. The first iteration used an Aumann DA3 with additional MK Automation aluminum framing to hold its position relative to the linear stage. Components for holding the wire reel were also created. The second version used an Aumann AS8 with mechanical feedback and built-in reel damper which controlled the wire tension.

The bobbins were held tightly in place with an expanding-sleeve mandrel which could expand up to 26.9 mm to hold a bobbin in place. The bobbin was pressed into the mandrel and the position was noted. G-code was written to coordinate the rotation of the 4^{th} axis and the movements of the linear stage such that a tighter coil can be achieved. The machine was programmed to complete all six layers at once. For co-wound wires, the machine was stopped when five rotations were complete and the carbon fiber tow was woven. Figure 13 shows the first and second iteration of the coil winding setup.

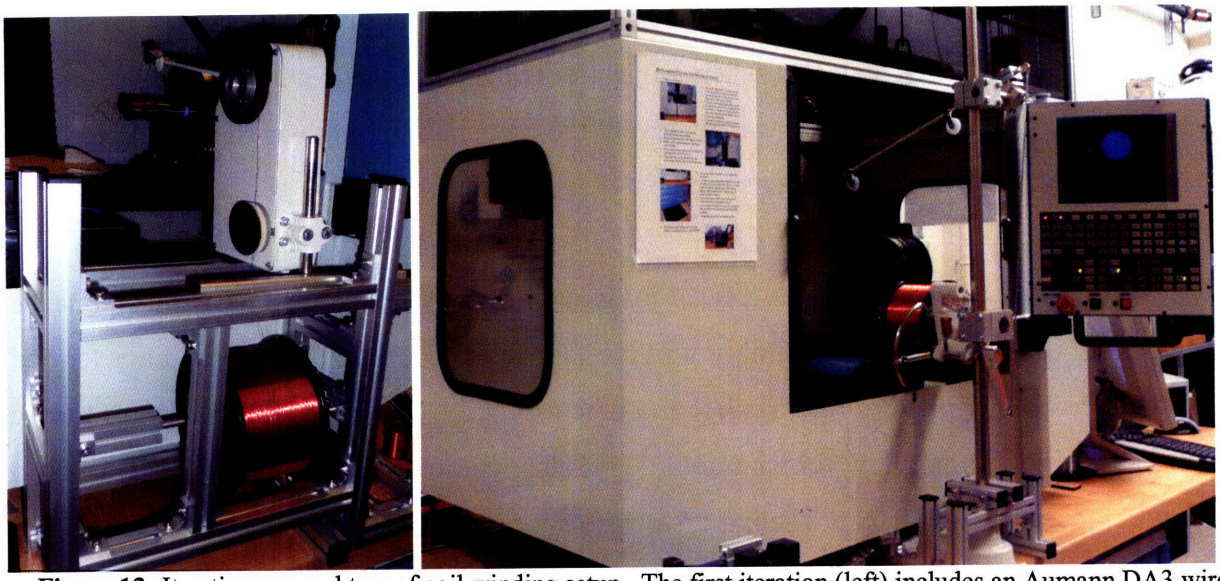

Figure 13: Iteration one and two of coil winding setup. The first iteration (left) includes an Aumann DA3 wire tensioner and an MK framing. The second iteration (right) includes an Aumann AS8 with mechanical feedback and built-in reel holder.

Due to the distance between the end of the wire tensioner and the tangent point on the bobbin, the program had to include linear stage movements which would shift an extra distance when the winding of the wire changed directions. Otherwise, the end of the wire tensioner would always lag behind the location on the coil where the wire was being wound onto. This procedure helped minimize spaces between wires in the coil. Depending on the speed of the 4^{th} axis, a coil can take as long as four hours to wind onto a bobbin.

3.2 Bobbin Manufacturing

The wet lay-up process was used to create the bobbin based carbon fiber tubes. The manufacturing process involves multiple steps and many different materials. The first concern for a tubular shape is that the inner form much both be easily removable, rigid, and could provide a smooth finish. An expanding sleeve mandrel was used for this purpose. The surface in contact with the carbon fiber during wet lay-up must be made of a material that does not bind with the laminating resin. The Frekote 770-NC releasing interface spray was used to help facilitate the release of coil and was sprayed in two separate coats on the former.

One of the practical concerns with using a mandrel is that the gaps that allow it to expand can cause wet carbon fibers to form into that shape. Therefore, another layer of 26 mm outer

diameter tubular material (polyethylene) was later used to serve as an intermediate interface. A slot was cut into the material so that when a mandrel is inside, the polyethylene tube would be fully expanded. When the mandrel was removed, the compliant tubing would be compressible allowing it to slip out of a carbon fiber structure.

Next, a layer of 6K carbon fiber was created by grouping many fibers together vertically at the desired length of the coil. This assembly was pre-fabricated to create the correct diameter and length and was then applied to the mandrel and tube assembly. The assembly was created to be longer than the bobbin to allow for trimming. This also required thick end caps to be added to the mandrel to extend its surface. Then, the 2-part Pro-set laminating resin (125 or 145 resin and 229 hardener) was mixed and applied to the surface. Because of the low viscosity of 450 mPa·s, wetting happens quickly and does not require compression or injection. A layer of release cloth is then added to the assembly. Originally, a woven fabric which allowed the resin to flow out was used. In order to create a better finish and to reduce the waste of resin, a high surface gloss release film was used. Lastly, the assembly was tightly sealed to maintain the tubular form. The assembly was then allowed to cure at room temperature for 15 hours. Figure 14 shows some of the materials used for the manufacturing process.

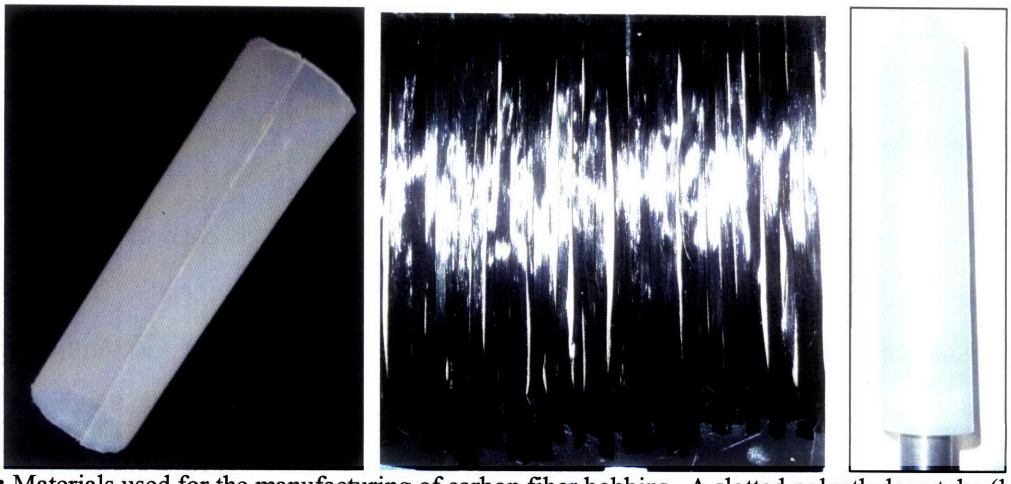

Figure 14: Materials used for the manufacturing of carbon fiber bobbins. A slotted polyethylene tube (left) is used to prevent ridging in the mandrel from appearing in the form of the bobbin. The unidirectional carbon fibers (middle) are first collected into a sheet before being applied to a surface. The release film (right) has a high surface finish is wrapped on top of the carbon fiber and resin.

After the material has cured, the release film, mandrel and inner polyethylene tube was removed leaving a bobbin with a fine finish. The carbon fiber tube is still in a malleable stage and can be

handled and cut down to the appropriate length. The top and bottom bearings are machined by first cutting them with a carbon dioxide laser for the finer details. The slots for carbon fiber attachment are the most difficult part to machine using conventional methods because of its thickness and depth. Next the electrical connections, potentiometer connection and linear guide hole are milled on a CNC machine. The carbon fiber bobbin is then attached to the top and bottom using the same laminating resin and cured at room temperature a second time. The assembly is then place in a high temperature vacuum oven for another 8 hours at 82 °C.

If the assembly is not properly cured at high temperatures, the laminating resin will settle into a brittle state which makes it ineffective. The laminating resin can be cured at lower temperatures for shorter period of time but for the maximum epoxy strength and temperature resistance, a longer curing time is recommended. Figure 15 shows the finished carbon fiber bobbin next to a plastic bobbin that was created in a computer controlled lathe.

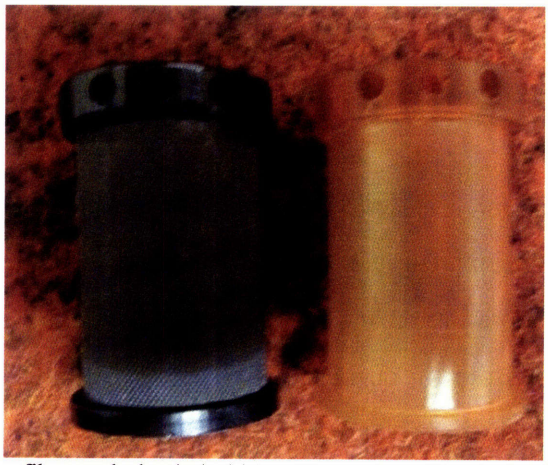

Figure 15: Comparison of carbon fiber and plastic bobbin. The carbon fiber bobbin (left) that is created by wet lay-up has similar dimensions as the plastic bobbin (right) created on a CNC lathe.

The entire process to create a bobbin starting from creating the 6K carbon fiber sheets from small segments of tow to lay-up and curing can take as long as 36 hours each (not including the time to wind the coil). In order to increase the production rate, two expanding sleeve mandrels were obtained.

3.3 Co-winding Manufacturing

For the bobbin design, the bobbin manufacturing process is separate from the coil winding process. Co-winding incorporates these two separate processes together into a new manufacturing technique. Considerations in creating a new winding technique need to have applicability in industry allowing coils to be manufactured in a reasonable time frame. One important concern for co-winding is that it may be more time consuming than creating a bobbin of the same material. Therefore the co-winding process must have similar manufacturing times as bobbin manufacturing. The goals are to:

- Minimize manufacturing time
- Maximize manufacturing rate
- Keep manufacturing and material costs low by reducing waste
- Ensure tight spacing in the copper for maximum current density per unit volume
- Use minimal material to hold the assembly in place before curing

Taking these ideas into account, a practical process for reducing the manufacturing time was created. First the top and bottom bearings were attached during the first application of epoxy such that a second room temperature curing stage was not needed. Second, the materials used to hold the carbon fiber in place during curing was reduced. Initially, thick disposable end caps were used to expand the length of the mandrel. To reduce the waste in the epoxy, carbon fiber, manufacturing time and the end caps, the carbon fiber length was made to be exactly the length needed to complete the winding such that the end caps and excess carbon fiber was not needed.

In the first co-winding stage, the polyethylene tube is placed onto a mandrel along with the bottom bearing and length markers are used to determine the start and finish for the coil. Next, 34 separate strands of 3K carbon fiber were cut to a length of 48 mm (each with a mass of 0.018 g) and color coded to differentiate odd and even strands. Next the lengths of carbon fiber tow were arranged with even spacing and in an alternating odd and even pattern. This pattern was then quickly transferred onto the mandrel and winding surface. First, the odd strands were lifted

away from the even strands and the copper was wound on top of the even pattern until five windings had passed. In order to reduce the stress in any particular area of the coil, the copper was over-wound by approximately 60 degrees such that transitions between the carbon fiber and copper did not always appear in the same vertical position on the coil.

Next the even strands are lifted away from the odd strands to such that the carbon fibers alternate in position. Then the copper is wound again. This process repeats twenty times until the fill length of the carbon fiber is created. Note that the only internal structure to the co-wound design is the carbon fiber and copper. At this stage, laminating resin is added to the carbon fiber structure. Even though the resin has a low viscosity, it can only penetrate approximately two layers of tightly wound copper coil. Therefore, the resin must be applied at least once every two layers. The next step is to wind pure copper four times along the length while impregnating the copper wire with resin.

Figure 18 shows the mandrel setup and a picture of the coil while it is being co-wound. Each carbon fiber tow is cut so that it is twice as long as is needed such that when the winding reaches the other layer, the same fiber cab used again.

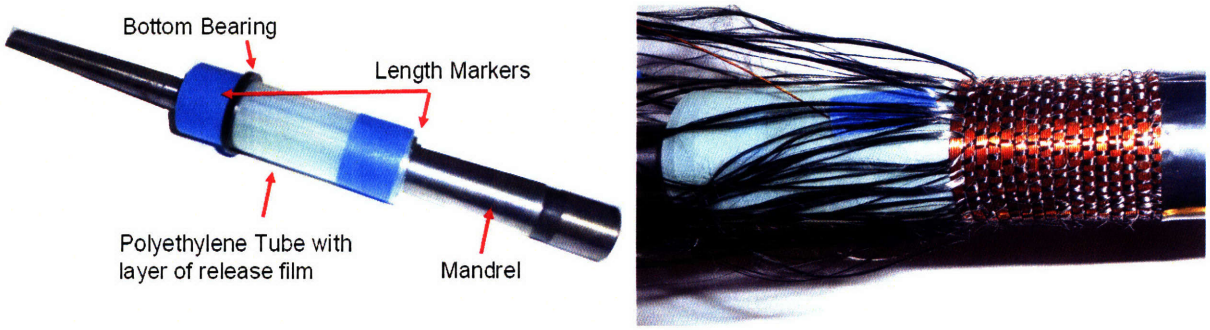

Figure 16: Mandrel setup and coil in the process of being wound. The mandrel setup (left) begins with the bottom bearing already attached. The co-winding process (right) uses carbon fiber strands that are twice as long as needed to create both the inner and outer windings.

At the end of the co-winding process, a thin layer of carbon fiber film with a weight of 0.029 g is used to cover the surface. This evenly distributes the laminating resin along the ridged co-wound surface. The assembly is removed from the mandrel and the labels are cut. The top bearing is incorporated and another layer of release film is added to provide a smooth finish. The assembly

is clamped and cured at room temperature for 15 hours. It is then cured at 82 °C for another 8 hours. Figure 17 shows the oven setup which can go as high as 300 °C.

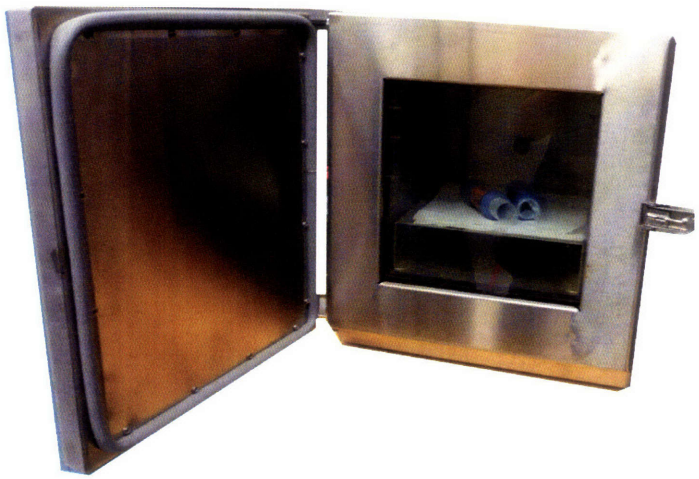

Figure 17: High temperature vacuum oven used to cure carbon fiber assemblies. Two carbon fiber co-wound coils are shown curing inside the oven.

After curing, the electrical connections are made and no other finishing steps are needed. The entire process minimizes the waste of carbon fiber, epoxy and other materials. Figure 18 shows one of the completed carbon fiber co-wound Lorentz force coils.

Figure 18: Finished carbon fiber and copper co-wound Lorentz force coil

The process also takes approximately six to eight hours to wind and a total of 32 hours to complete making it comparable to the time to build a carbon fiber bobbin. One of the advantages is that the top and bottom bearings are incorporated during the winding process which helps create a tighter bond between the bearings on the coil itself. The current plastic bobbin coils

have a mass of 51.8 g while the co-wound coils have an average mass of 48.0 g. On average, the coils are 3.75 ± 0.155 g lighter than the current coils with plastic bobbins even when co-wound coils have additional laminating resin in the gaps between the copper wires.

4. Characterization

In order to validate that the design does provide benefits, many tests were conducted on the new material to determine is properties and to see if it differs substantially from the original plastic bobbins. The electrical impedance of the material is analyzed both in free air and with the magnetic field crossing the coil. Next a heat transfer model is presented and compared to actual data. Small temperature sensors were placed to the inner and outer surfaces of the coil inside the air gap in order to obtain temperature data. This coil heating times were determined for the coil both inside and outside the steel casing. Dynamic mechanical and compression strength testing was also conducted to verify the strength of the co-wound coils to show that they do outperform bobbin-based designs.

4.1 Impedance Analysis

At lower frequencies, a coil of wire acts like a resistor with an approximate resistance of 12.5 Ω. At higher frequencies, the coil begins to act like an inductor and at even higher frequencies, the impedance amplitude and phase of the inductor begins to oscillate. The HP 4194A Impedance/Gain Phase Analyzer was used to collect information from the coils. This information was then passed through a HPIB bus on to a computer using a National Instruments GPIB-USB-HS connector. The data were then collected through LabVIEW 8.5 in a VI originally created by Chris Bae. The impedance was found from multiple locations inside the coil because as more of the coil is immersed in the magnetic field and the exposed to electrically conductive materials, the impedance of the material will change causing a varying electrical response at different locations inside the steel casing. Figure 19 shows a picture of the experimental setup and a block diagram indicating the different instruments used to obtain data.

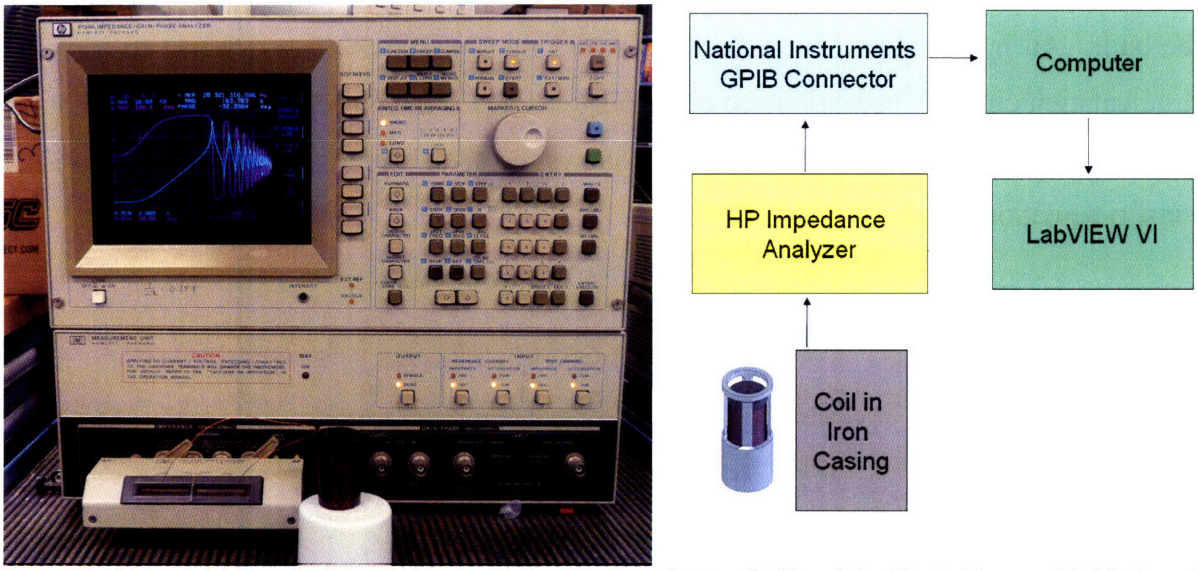

Figure 19: Instrumentation for Impedance Analysis. The actual setup (left) and the block diagram (right) show the setup for the analysis including an HP Impedance Analyzer, a National Instruments connecter through a computer which has a LabVIEW VI (originally created by Chris Bae) which reads and stores the data.

In order to run a test, the impedance analyzer is first set to the desired gain-phase plots, next it is synchronized with the LabVIEW VI. As the impedance analyzer sweeps through different frequencies, the VI records one full sweep and saves the data into a text file.

4.4 Heat Transfer Analysis

Heat transfer plays a big part in the power handling capabilities of a Lorentz Force coil. At high voltages and current, the coil quickly heats up quickly causing failure by burnout. Carbon fiber co-winding can potentially reduce this problem because the carbon fiber has higher thermal conductivity than polysulfone or other plastics. In addition, the thermal conductivity of laminating epoxy is an order of magnitude higher than that of air which helps move the heat away from the copper coils and distributes the temperature more evenly.

Coil heating goes as the current squared and a coil could overheat in less than a second if ten amps or more was applied to it. Therefore, in order to prevent the test setup from burning out the coil and to keep the temperature time scales to a reasonable level, a lower voltage supply of 15 volts at 7 A to 30 volts at 4 A was selected. The power supply used was an HP E3632A.

To collect information on the temperature of the coil, an electronic setup and a LabVIEW VI had to be built. An independent low current power supply (HP 3631A) was selected to power the instrumentation circuitry because noise could be generated if the power supply to the coil and to the instrumentation was the same. Figure 20 shows the actual setup and the block diagram for the instrumentation.

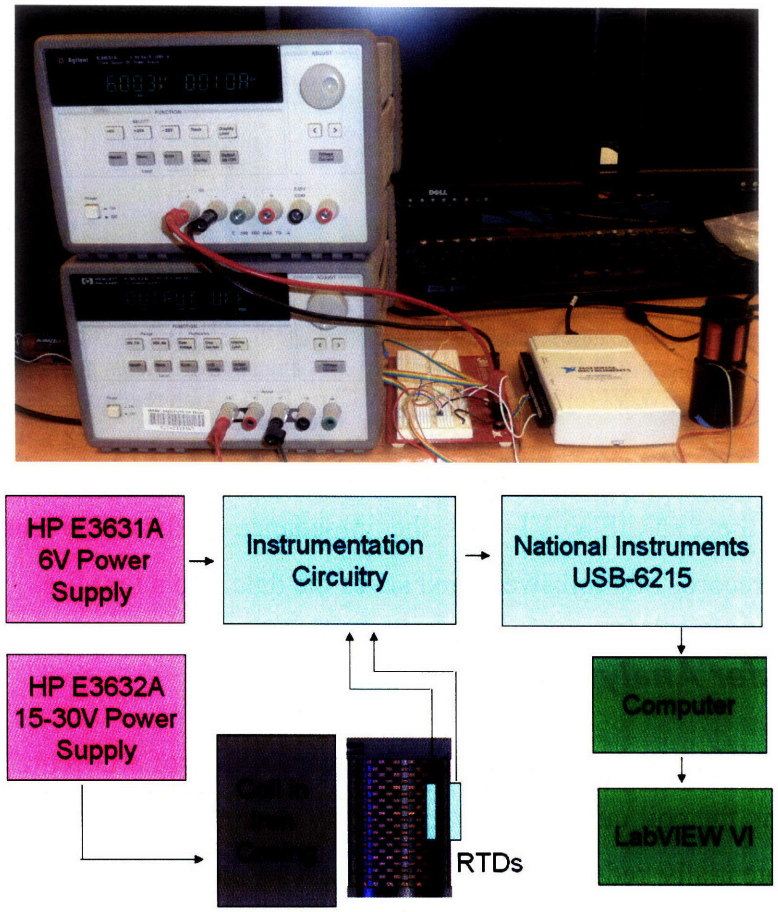

Figure 20: Instrumentation for temperature analysis. The actual setup (top) and the block diagram (bottom) show how two separate power supplies are used to send power to heat the coil and to collect and store temperature information in the LabVIEW VI.

Small platinum film resistance temperature detectors (RTDs) with a model number F2020-100-B from Omega (Class B accuracy with a ± 0.12 °C resistance tolerance) were chosen. These RTDs have a small dimension of 2 mm × 2 mm with a thickness of less then 0.8 mm. The top glass coating can be easily sanded down to help it fit inside the air gap between the coil and the walls of the steel casing. Although the air gap between the coil and the outer wall is sufficiently large enough for an RTD to fit inside, the gap between the magnet and the inner wall of the coil is not sufficiently large. Therefore, the magnetic core of the steel casing was removed and replaced with a stainless steel core with a slot cut into it that is slightly larger than the size of the RTD.

Stainless steel has similar thermal properties (conductivity, heat capacity and thermal diffusivity) as the Nd-Fe-B magnets. Without magnets inside the coil, when a force is applied, the coil will not move thereby reducing the risk of RTDs being broken during the heating process.

The RTD sensors also have a fast response time that is equivalent or better than similar wire wound elements [28]. Each RTD is adhered to the surface of the coil using Omega OB-101-2 thermally conductive epoxy which can handle high temperatures. The RTDs are measured by connecting them in series with 1.5 kΩ resistors and information is collected on a National Instruments NI USB-6215. Figure 21 shows the LabVIEW VI and the user interface created for this setup.

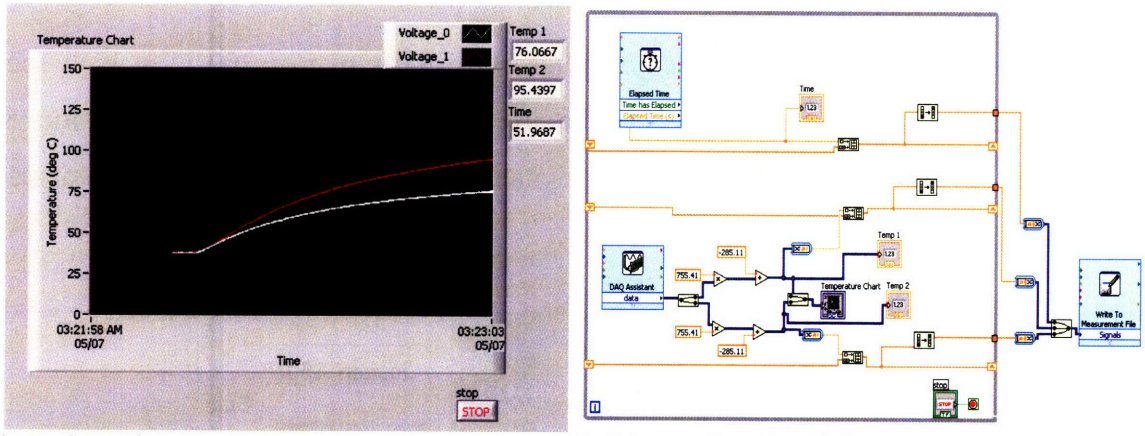

Figure 21: LabVIEW program for Temperature Analysis. The user interface (left) and LabVIEW 8.5 program (right) collects and stores the temperature data.

A LabVIEW 8.5 VI was built to calibrate and collect information from the sensors and to save the data. The sensors were calibrated at a supply voltage of 6.0 V. Next, the calibration constants were entered into the program. In order to run a test, the power supply for the sensors was first turned on and then the VI was started. A few seconds is used to determine if the temperature was in the correct range and then the power supply for the coil was turned on and the temperatures for both sensors was recorded up to a temperature of 140 °C or when the recorded temperature seemed to reach a steady state. The original plastic bobbin coil and the carbon fiber copper co-wound materials were tested at 15 V and 30 V both inside the steel casing and in free air.

4.3 Dynamic Mechanical Analysis and Compression Strength

The strength of carbon fiber is much higher than that of any metal or plastic. Of the two types of loads, tension and compression, carbon fiber is weakest in compression with a quoted compression strength of approximately 2.06 GPa which is 58.9 % of the tensile strength [4]. However, after undergoing the winding process the fibers are held in tension and sometimes broken; this makes the expected compression strength is much lower. In addition, when the coil is in compression, modes of failure include not only buckling of the carbon fibers but cracking in the epoxy, manufacturing defects or lateral displacement by the copper coil. The most realistic situation in the high force NFI case is compression between an area of the coil and the piston. The worst case scenario is when the force is applied to the very bottom of the coil.

Most of the time, the coil will be undergoing forces in the range of 200 N at high speeds. Therefore, dynamic mechanical testing can be used. Figure 22 shows the Instron 8501 instrument and control pad used to conduct dynamic mechanical testing and compression strength testing.

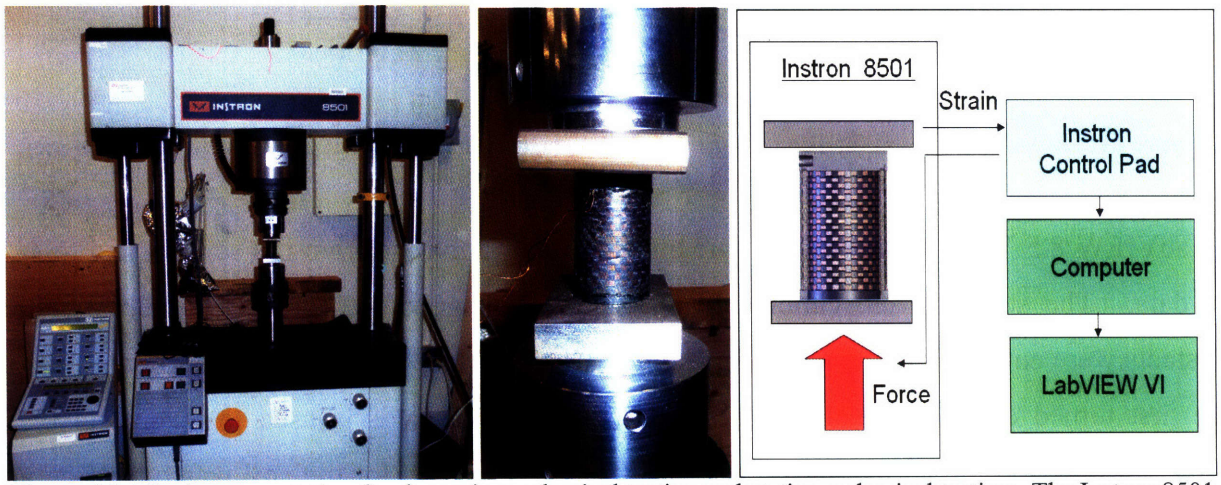

Figure 22: The instrumentation for dynamic mechanical testing and static mechanical testing. The Instron 8501 (left) was used to test the coils as they sit between two platens (middle). The block diagram of the instrumentation illustrates the flow of information (right).

The Instron is capable of operating up to ± 100 kN dynamic which is well outside the strength of the coils. Each coil is placed between two steel platens to ensure that load is applied evenly. A control pad is used to control the hydraulics, forces, and strains and outputs to a LabVIEW bus

from which a VI could read the information. The design for the LabVIEW VI used for the dynamic and static testing is shown in Figure 23.

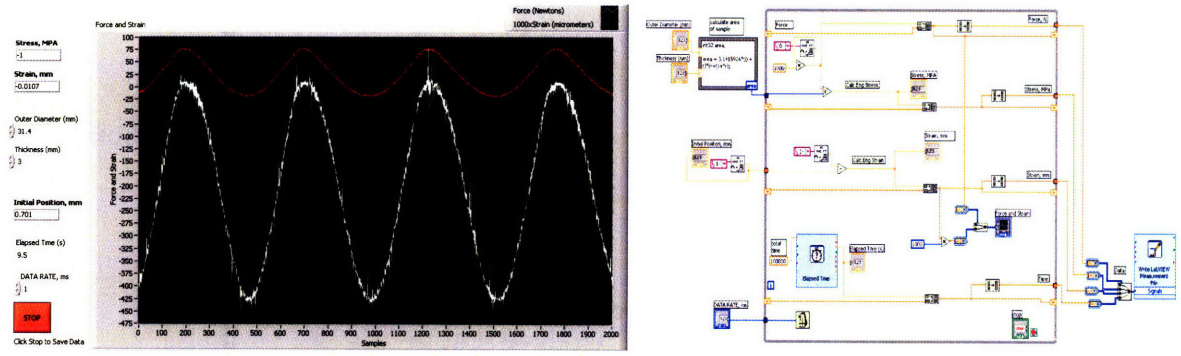

Figure 23: Dynamic mechanical analysis and compression strength analysis LabVIEW VI. The user interface (left) displays the forces and strains (multiplied by 1000) on the graph. The program (right) collects the data, displays it, and stores it in a text file.

The process for dynamic mechanical testing involves turning on the hydraulics to a high stage and controlling the position of the platens so that a sample can be loaded in the center. Then, the position is controlled until the sample is in compression. Then, a preload is applied to the sample that is at least 10 to 100 N above the actuation amplitude. The tests are isotonic forcing the machine to provide a given force and to measure the strain. The isotonic forces amplitudes used were 50, 100 and 200 N. The frequencies of oscillations used were in the range of 0.1 Hz to 100 Hz. The Instron 8501 machine is unable to complete a high frequency oscillation without losses in the amplitude. The proportional gain (Kp from 10 to 20) of the instrument was adjusted to help with this situation. The coils tested were the original plastic bobbin coils, carbon fiber bobbin coil, free standing copper coils, and carbon fiber copper co-wound coils.

The process for compression strength testing involves the same insertion steps and preloading steps. Then the material is loaded with force increments of 0.1 kN and held for approximately 20 seconds to measure the creep. One of the important aspects of buckling is that the buckling load of a constant force is much lower than the buckling load of an instantaneous force. For viscoelastic and composite materials, creep can cause fracture at lower loads as different parts of the coil begin to fail. The load at which failure occurred is recorded along with the stress and strain outputs. The materials tested were the original plastic bobbin coils, freestanding copper coils and carbon fiber copper co-wound coils.

5. Results and Discussion

5.1 Impedance Analysis

The impedance was analyzed both outside the steel casing and inside the steel casing. The data was collected and the impedance for the three different types of coils, the plastic bobbin coil, the carbon fiber bobbin coil and the co-wound coil, are shown in Figure 24.

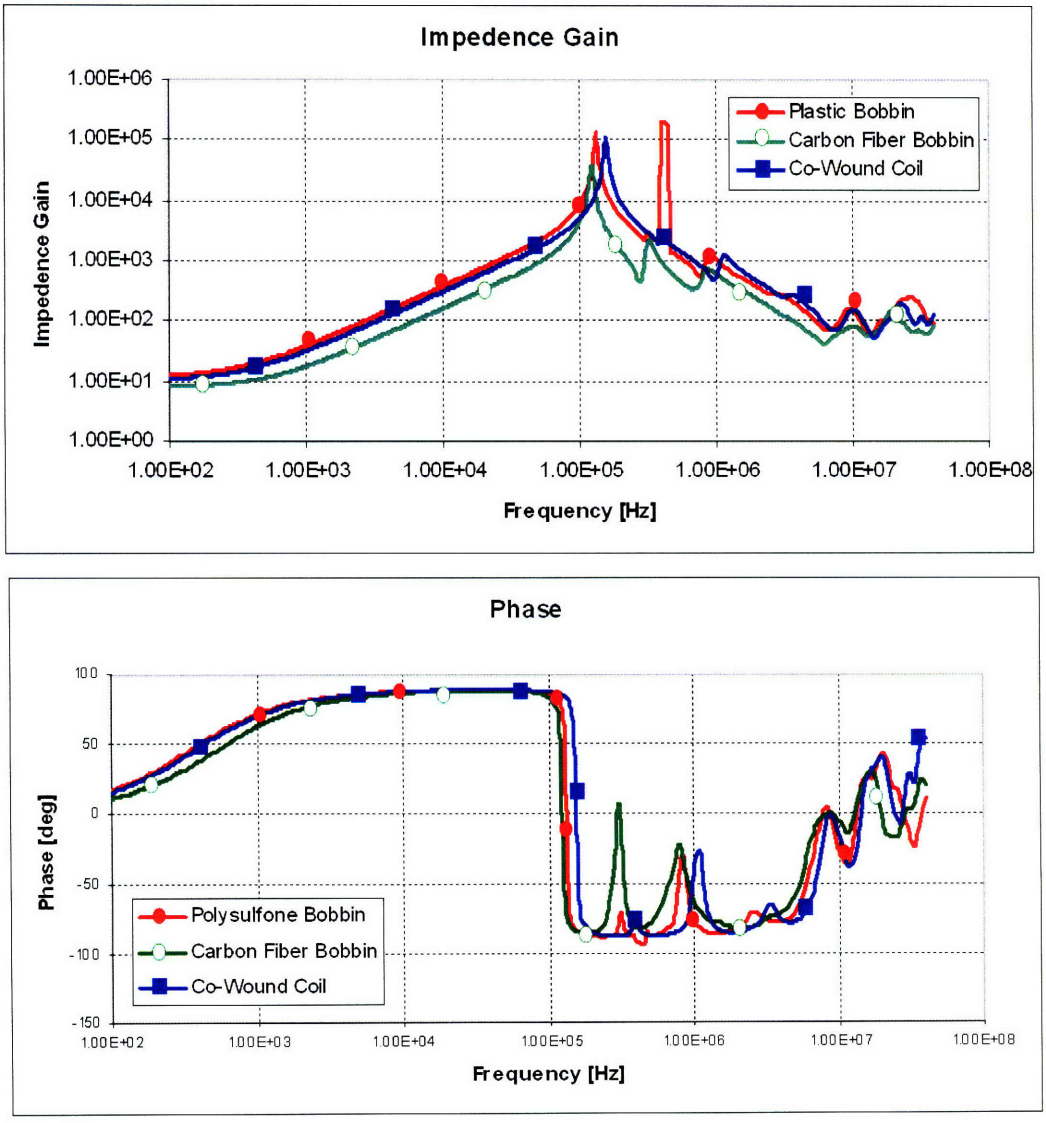

Figure 24: Gain and Phase information for three different types of coils.

From this figure, it can be concluded that the plastic bobbin coil and the co-wound coil are extremely similar even though the co-wound coil has extra gaps in it due to the transition regions in the carbon fiber. Up to approximately 150 kHz, the coils seem to act like a simple RLC circuit with a resistor and inductor in series with a capacitor in parallel with the two. The impedance for this type of configuration is,

$$Z(s) = \left[\frac{1}{(R + Ls)} + Cs \right]^{-1} \quad , \tag{5.1.1}$$

where Z is the impedance as a function of s, R is the resistance, L is the inductance and C is the capacitance. This function can then be used to do a curve fit to determine the equivalent resistance, inductance and capacitance of the circuit at lower frequencies. The best fit for the gain and the phase produced a resistance of 12.8 Ω, an inductance of 6.2 mH and a capacitance of 200 pF for the original plastic bobbin coil.

Next, the coils were subjected to different levels of emersion into a magnetic field and their positions were recorded with the linear potentiometer. The plot for the co-wound coil is shown in Figure 25. As the coil is placed more and more into the magnetic field and more of the coil is exposed to electrical conductors, the peak impedance magnitude becomes smaller and the circuit becomes less like an RLC circuit. The largest changes are in the middle frequency ranges where the peak impedance magnitude drops from 10,000 to 1,600 while the frequency for peak gain increases.

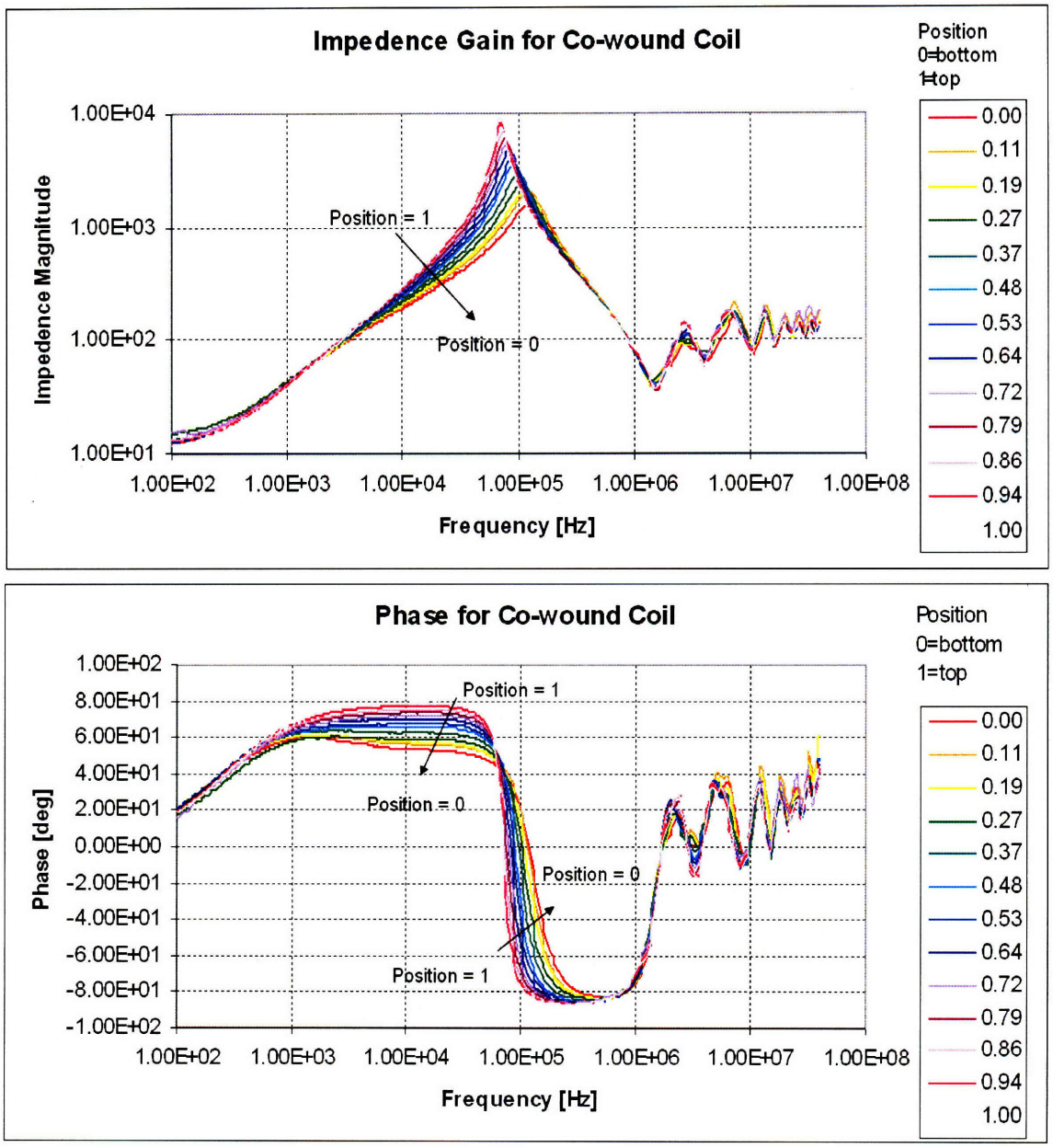

Figure 25: Gain and phase as a function of the vertical position of the co-wound coil. A position of 0 means that the coil is at the very bottom of the steel casing and magnetic core while 1 means that it is at the top or the maximum distance away from the magnetic field.

In the phase, the coil with a position of zero has a very distorted phase in middle frequencies and as the coil is moved up, the phase becomes more like an RLC circuit. There is very little difference at high frequencies and at low frequencies indicating that the components that seemed to have been affected by the introduction of the magnetic field and the conductor are nonlinear changes to the inductance L and the capacitance C while R and other higher frequency variables did not change.

5.2 Temperature Analysis

5.2.1 Comparison of Free-Air and In-Casing Temperatures

The temperature profiles for both the original plastic bobbin coil and the co-wound coil are compared. The graphs for the temperatures at different applied voltages for temperature sensors placed on the coil while it was standing in free air and in the air gap are also plotted together. Figure 26 shows the different temperature distributions after an input voltage is applied.

The graphs indicate a few important aspects. One of the first aspects to note is that for any time on the graph, the temperature for the carbon fiber materials is higher than for the polysulfone. Although the co-wound coil has a slightly lower resistance than the original polysulfone coil the effect is still significant after adjusting for the differences in resistance. Therefore the transient temperature difference can be attributed to better transient heat transfer for the co-wound coil.

In the transient, the temperature depends on the amount of heat flow out of the copper as current goes through it. As the heat transfer increases due to better material selection, less of the heat generated by the current is kept inside the coil and more of it is transferred out of the coil into the ambient air or into a steel casing or the internal magnets. In general, a higher temperature indicates better heat transfer.

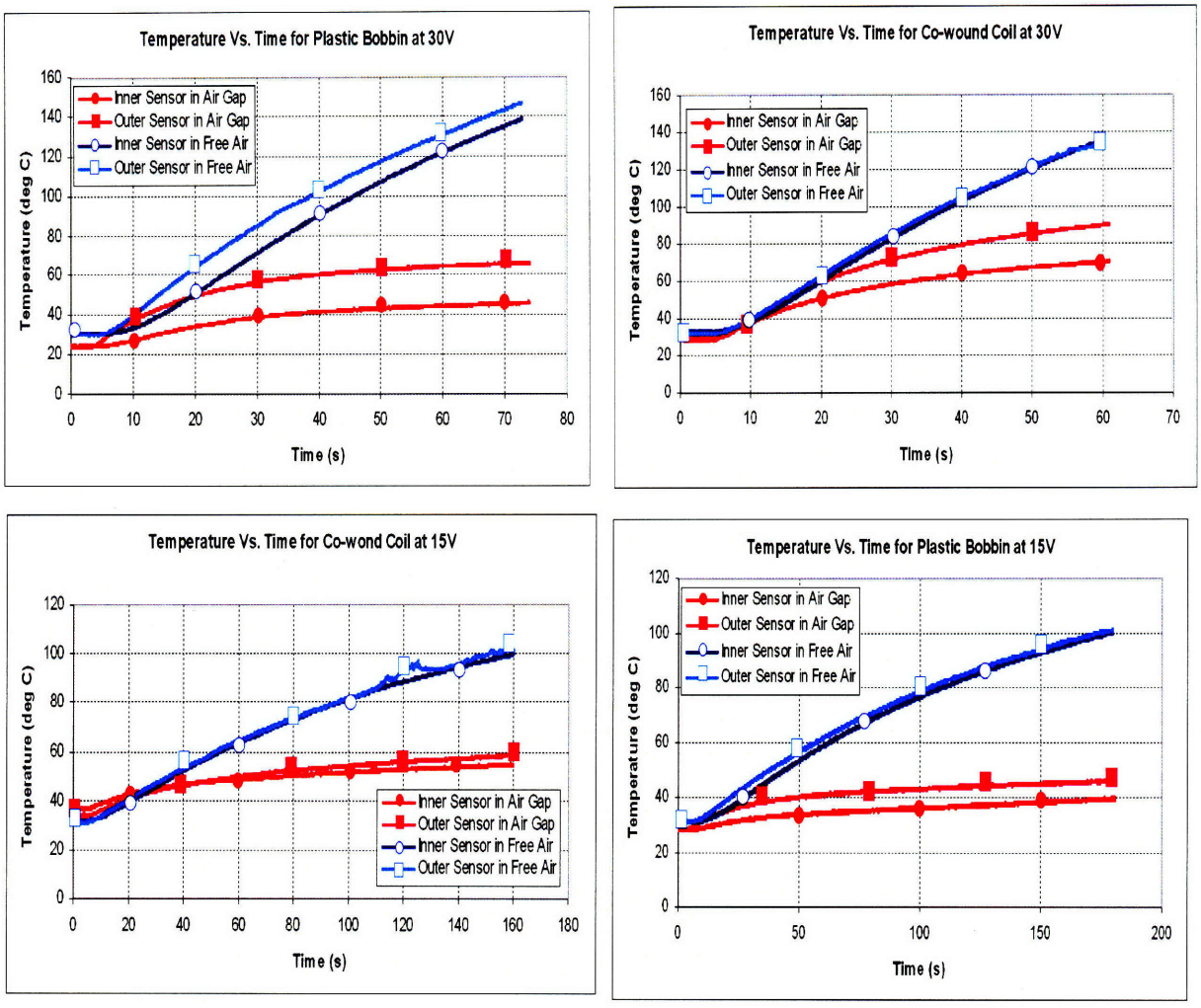

Figure 26: Temperature profiles of the original polysulfone and the co-wound coil. The polysulfone (2 graphs on the left) and the co-wound coils (2 graphs on the right) show different temperature characteristics when 30 V (2 graphs on the top) and 15 V (2 graphs on the bottom) are applied.

Another interesting aspect is that the outer temperatures are always greater than the inner temperatures. This is mainly because the outer surface area is larger. In the case of the polysulfone, the temperature gap between the inside and the outside tends to be larger indicating that the difference between the heat transfer ability of the inside and the outside is much higher. This is mainly due to the bobbin. Polysulfone has a conductivity of 0.218 to 0.600 W/mK depending on the manufacturer. Since the co-wound coil does not have a bobbin or is in contact with high conductivity carbon fiber directly in contact with the air gap, there is minimal difference between conductivity per unit area of the inside and the outside when dealing with a co-wound coil. Therefore, in the coil that was exposed directly to the air, the temperature

difference between the inside and the outside is almost zero. For the profiles obtained in the air gap, the temperature differences for the carbon fiber are smaller than for the original bobbin form.

Although only the temperatures at the outer and inner surfaces can be assessed, the highest temperatures occur in the middle of the coil. This is because each segment of copper wire receives the same current so that each segment generates the same heat. The outer sections near air gaps or the ambient air can transfer heat through conduction or natural convection to restrain self heating. The coils in the center, however, are unable to do this and therefore achieve higher temperatures than neighboring segments which have access to a lower temperature reservoir. Therefore the temperatures measured in this experiment are the minimum temperatures of the coil and do not indicate how high the maximum temperature of the coil can get.

5.2.2 Free-Air Model

The temperature and heat transfer effectiveness of each type of coil can be modeled and verified by the data. The most important case is when the heat transfer out of the coil is weak and the coil is more likely to fail due to burnout. This is the case for when the coil is in free air.

The model for determining the heat transfer is derived using the first law of thermodynamics and a control volume around the coil. The change in energy inside the coil is found to be equal to the difference between the rate of heat being generated by the coil and the rate of heat lost to the atmosphere. The ratio of the diameter of the bobbin to its thickness is 0.023 which means that the outside and inside of the coil can be approximated as a flat plate which can be used to model the natural convection. In natural convection, the hotter and less dense air rises vertically creating a boundary layer. The result for a control volume around the copper coil portion of the assembly is,

$$\frac{dE}{dt} = Q_{in}(t) - Q_{out}(t) \ , \qquad (5.2.1)$$

where the *dE/dt* term is the change in energy of the copper, topcoat and air, $Q_{in}(t)$ is the heat that is transferred into the coil and $Q_{out}(t)$ is the energy transferred out of the coil to the environment.

The overall heat transfer coefficient is composed of the different resistances. It was found that conduction through the topcoat of the coil, conduction through the plastic bobbin and convection dominate the heat transfer.

Many transient heat transfer models are available when multiple modes of heat transfer exist in a system. The Biot number is used in many situations to determine the appropriate model. The Biot number is defined as $Bi = Ut_{coil} / k_{coil}$ where Bi is the Biot number, U is the overall heat transfer coefficient which incorporates the heat transfer due to conduction and convection and t_{coil} is the thickness of the copper coil and k_{coil} is the conductivity of the coil. When the Biot number is much smaller than unity, the thermal gradient will be in the fluid which indicates that there will be virtually no temperature gradient in the solid material such that there is a semi-uniform temperature distribution in the coil.

In order to determine the magnitude of the overall heat transfer coefficient, conduction and convection must be analyzed. The conductivity through the topcoat, the bobbin and carbon fiber which are all configurations for the coil assembly in free air,

$$R_{topcoat} = \frac{d_p}{k_p A} + \frac{d_{ai}}{k_{ai} A}, \tag{5.2.2a}$$

$$R_{bobbin} = \frac{d_{bobbin}}{k_{bobbin} A}, \tag{5.2.2b}$$

$$R_{CFt} = \frac{d_{CF}}{k_{CF} A} + \frac{d_{resin}}{k_{resin} A}, \tag{5.2.2c}$$

where R, resistance associated with each type, is a function of the thickness d of each material divided by the conductivity of the material and the total area covered by the material A in either the inner surface or the outer surface. The resistances can be added to obtain a total conductive resistance from the heat source (copper) to the convective surfaces.

The natural convection can be used to calculate the convection from the inner and outer surfaces of the coil. Since the coil is not maintaining a constant temperature, the normal Rayleigh number for vertical plates cannot be used. Rather, a modified version of the Rayleigh number which is

no longer a function of temperature can be used and iteratively solved. The Rayleigh number suggested by Lienhard [29] is,

$$Ra = \frac{g\beta q_w x^4}{kv\alpha}, \tag{5.2.3}$$

And the Nusselt number associated with this Rayleigh number is,

$$Nu = \frac{0.73(Ra)^{1/3}}{[1+(0.492/\mathrm{Pr})^{9/16}]^{16/45}}, \tag{5.2.4}$$

where Ra is the Rayleigh number, g is the gravitational constant, α is the thermal diffusivity of air v is the ratio of the viscosity to the density of air, and x is the effective height of the coil. The coefficient of thermal expansion β for air modeled as an ideal gas is equivalent to $1/T_{ref}$ where T_{ref} is a reference temperature. Gas properties are also evaluated at this reference temperature defined as $T_{ref} = T_w - 0.83(T_w - T_{amb})$. This equation is valid for the ration of T_w/T_{amb} (in Kelvin) between unity and three. Here, T_{amb} is the ambient temperature and T_w is the wall temperature of the coil. The value q_w is the heat being transferred out of the coil and is iteratively solved for. The Nusselt number is Nu and the Prandtl number is Pr. The ranges of these values are checked to fall within reasonable bounds for the correlation.

The heat transfer coefficient due to convection is defined as $h_{conv} = Nuk_{air}/A$ so that the resistance due to convection is determined to be $R_{conv} = 1/(h_{conv}A)$. To determine the overall heat transfer coefficient,

$$U_{bobbin} = \frac{1}{A\sum R} = \frac{1}{A}\left[\frac{1}{R_{conv,out} + R_{topcoat,out}} + \frac{1}{R_{conv,in} + R_{topcoat,in} + R_{bobbin,in}}\right], \tag{5.2.5}$$

$$U_{CF} = \frac{1}{A\sum R} = \frac{1}{A}\left[\frac{1}{R_{conv,out} + R_{topcoat,out} + R_{CF,out}} + \frac{1}{R_{conv,in} + R_{topcoat,in} + R_{CF,in}}\right], \tag{5.2.6}$$

are used for the bobbin case and for the carbon fiber case in free air. Since both the inner and outer surfaces dump the heat into the ambient air, these two resistances are in series. For each of the resistances, the first subscript is the referenced resistance equation and the second subscript (in or out) is the reference area. To verify that this model can be used, the Biot number is calculated and the average Biot number on the inside is 2.55×10^{-4} and the average Biot number

on the outside is 3.08×10^{-4}. The average overall heat transfer coefficient was found to be range from 6.19 to 45.59 depending on operating conditions and power input to the coil.

The Biot number values indicate that a modified lumped capacitance model could be used to analyze the transient heat transfer behavior. With this model, the heat capacity of the wafer can be assumed to be constant at any time t. The density ρ, volume V and heat capacity c_p of the copper, topcoat and interstitial air (or resin and carbon fiber) can be approximated as constant over the process such that,

$$\frac{dT_w(t)}{dt}\sum(\rho Vc_p) = P_{in} - UA(T_w(t) - T_{amb}), \qquad (5.2.7)$$

where this equation is a first order linear ordinary differential equation which can be solved for Tw as a function of time. By guessing a solution with an exponential form and using the initial condition $T_w(t=0)=T_{winitial}$ and by solving for the homogeneous and particular solutions, the equations,

$$T_w(t) = \frac{C_2}{C_1} + (T_{winitial} - \frac{C_2}{C_1})e^{-C_1 t}, \qquad (5.2.8)$$

$$C_1 = \frac{UA}{\sum(\rho Vc_p)}, \qquad (5.2.9)$$

$$C_2 = \frac{Pin}{\sum(\rho Vc_p)} + \frac{UA}{\sum(\rho Vc_p)}T_{amb}, \qquad (5.2.10)$$

can be derived. The theoretical model can be compared to experimental data by graphing both with respect to time. This method gives the temperature on the outer and inner sides of the copper or copper and carbon fiber coil. However, it does not give information on the temperature of the plastic bobbin. The plastic bobbin has a much larger Biot number of 0.16; however, it can still be reasonably approximated as a lumped capacitance. The same analysis as completed for the control volume of the coil is also completed for the control volume of the bobbin.

The temperature on the inner surface of the bobbin will lag the temperature of the coil by a few seconds initially because the Fourier number $Fo = \alpha_{bobbin}t/d_{bobbin}^2$ is very small. The bobbin in a

short time period can be seen as an infinite slab with a characteristic time shown in equation 5.2.11 [29].

$$t_{lag} = \frac{d_{bobbin}^2}{\zeta^2 \alpha_{bobbin}} \tag{5.2.11}$$

In this equation, the lag time between when the bobbin temperature responds to a change in the coil temperature can be found by the thickness of the bobbin, the thermal diffusivity of the bobbin and $\zeta = x/(\alpha t)^{1/2}$ which is a dimensionless number. From tables in [29], the value for when the temperature difference of the bobbin responds by 50 % of the temperature change in the coil is found to be $\zeta = 1.013$ which is then used to calculated the temperature lag. The code for this analysis is shown in the appendix and results are displayed in Figure 27.

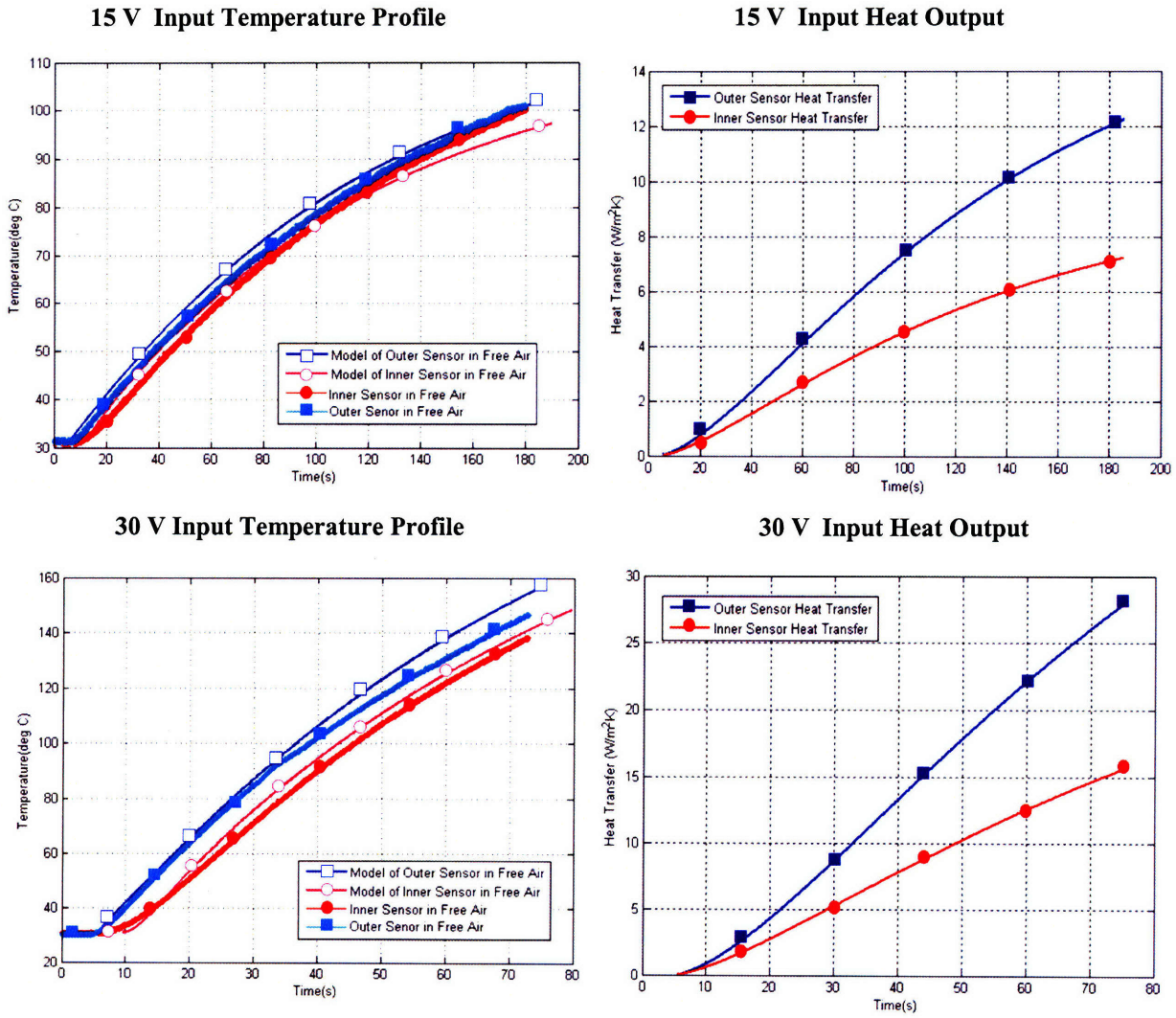

Figure 27: Original plastic bobbin based coil temperature and heat simulations along with actual data for 15 V (top) and 30 V(bottom) .

The temperature simulations show similar profiles to the temperatures achieved by the actual coil. The error between the model and the actual data can be from a few sources. First, the error can come from the thermal contact between the sensor and the surface of the coil. Secondly, the sensors have a thermal mass which may distort the results slightly at the beginning. For the 30 V and 15 V case, note that the inner sensor is converging to the temperature of the outer sensor which is not seen in the simulations. This may be due to the fact that the simulations do not capture the fact that the air inside the bobbin is constrained from moving by the small size of the ventilation holes. This causes the air to heat up such that the surface is no longer transferring heat to the ambient. The model does not account for this effect. Another source of error is that as the coil heats up, the resistance increases and the current decreases which may cause the model to over-predict the heat generation of the coil thereby over-predicting the temperature. The error in the 15 V model ranges from 2 % up to 4 % while the error in the 30 V model ranges from 1 % to 9 %.

The model also outputs information about the heat transfer out of the coil. The heat transfer of the outer surface is much larger than the heat transfer out of the inner surface mostly due to the resistance of the bobbin. In fact, heat transfer is on average 1.71 times better for the outside than the inside.

This same model can be used to calculate the profiles for a carbon fiber coil at 15 V and 30 V. The main difference is that the co-wound bobbin does not contain the thick insulation of the bobbin but makes up for this area with an approximately equivalent volume of carbon fiber and laminating resin. The laminating resin also fills the interstitial spaces between the wires replacing air in the earlier model. Plots from this model and from experimental results of the co-wound coil in free air are shown in Figure 28.

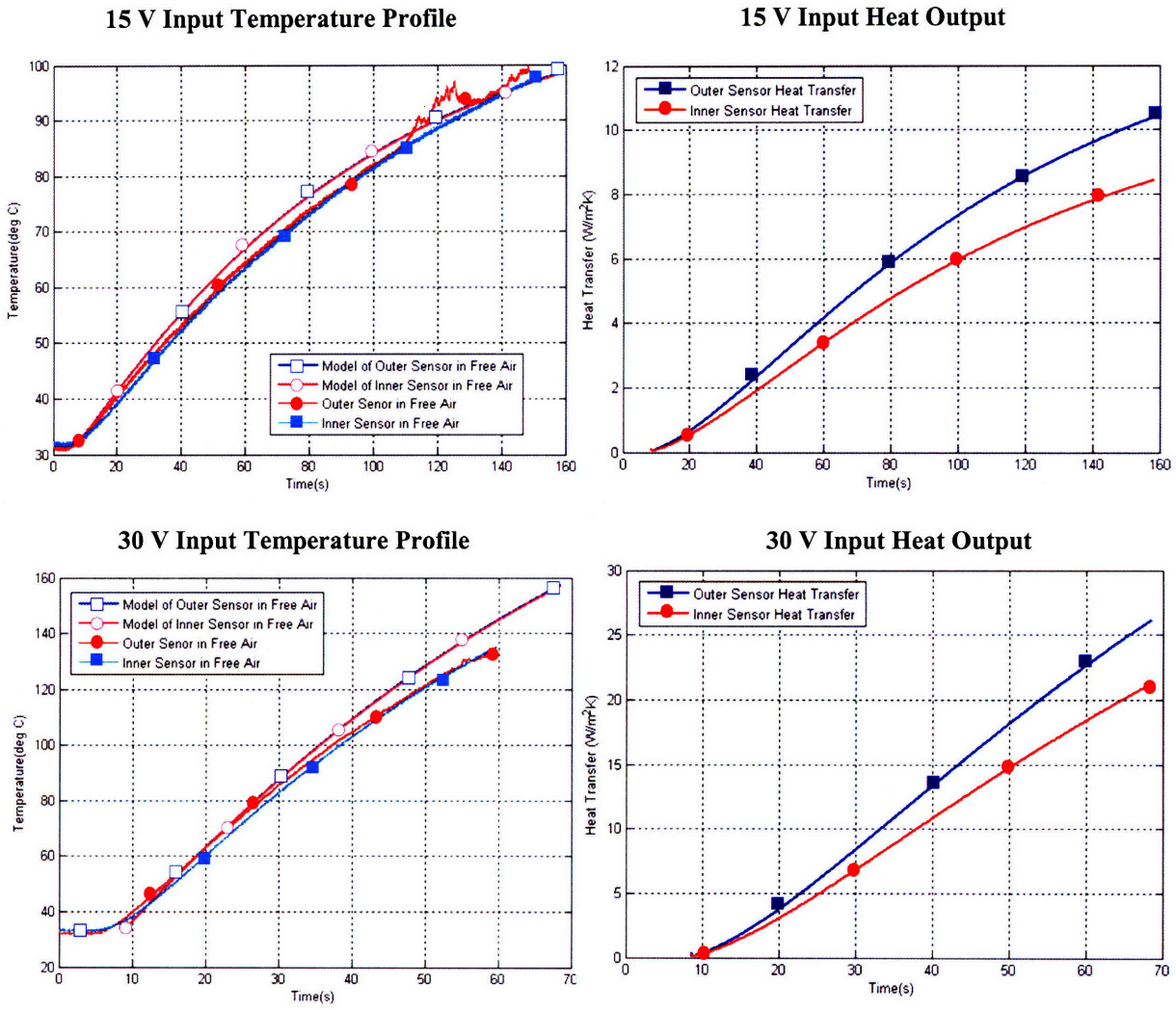

Figure 28: Co-wound coil temperature and heat simulations along with actual data for 15V (top) and 30V(bottom) .

Because the inner and outer layers of the coil are composed of the same materials as the outer layers of the co-wound coil, the temperatures for both are very similar as can be seen in the simulation and for the actual data. In fact the model's inner and outer temperatures are so similar that they lie on top of each other. For the data collected, the inner and outer sensors show a slight difference in their temperatures which may be due to differences in contact or calibration. The model over-predicts the temperature for the 30 V case and the 15 V case with error as high as 8.5 %.

One of the most important things to notice is that the heat transfer in the co-wound coil is higher overall that the heat transfer in the plastic bobbin coil. The inner heat transfer for the co-wound coil is 18 W/mK at 60 seconds in the 30 V case while for the plastic bobbin coil, the heat transfer

is only 12.5 W/mK. The corresponding outer heat transfer is 22.5 W/mK for the co-wound coil and for the plastic bobbin coil. This means an average increase in heat transfer of 15.7 % which is significant considering the only change was shifting from a bobbin to a co-wound structure with no additional forced convection or fluid cooling.

This model can be applied to higher voltages to determine the time at which the coil will reach a critical temperature. The co-wound coil at 200 V reaches 200 °C at 0.97 s while the plastic bobbin coil reaches this temperature at 0.76 s. The co-wound coil at 200V reaches 240 °C at 1.2 s while the plastic bobbin coil reaches this temperature at 0.94s. This gives the controller an extra 0.21 to 0.26 seconds to respond to a critical temperature. This extra time can be important if a temperature monitoring system has a time lag or the sensor has a large thermal mass.

From these results, it can be concluded that the carbon fiber co-wound material transfers heat better than the original plastic bobbin. This fact can help reduce thermal burn-out of the coils and provide an earlier indication to any temperature limit sensors that the maximum temperature inside the coil is at an unacceptable level.

5.3 Dynamic Mechanical Analysis

The coils were tested between 0.1 Hz and 100 Hz. At each of these intermediate frequencies, the strain (displacement) response is recorded and a set of results for a carbon fiber bobbin is shown in Figure 27. The graph shows the response at 2Hz with input amplitude of 200N. Note that compression is noted in the negative direction.

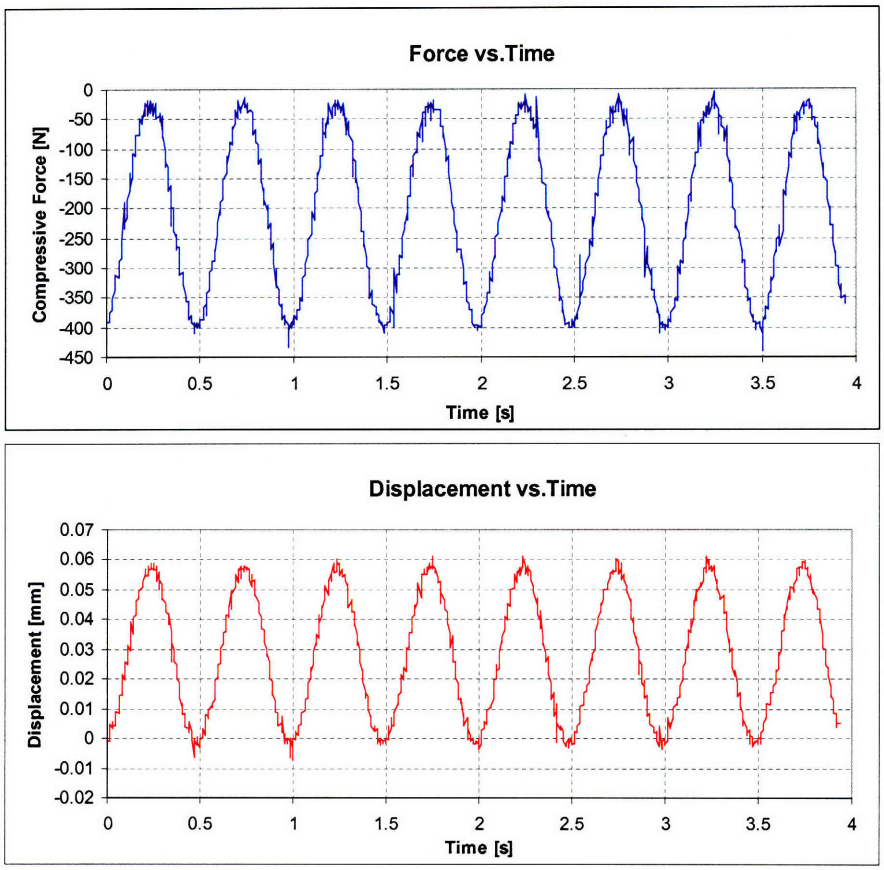

Figure 29: Force and displacement in an isotonic test on a carbon fiber bobbin. The material is actuated at 2Hz with a preload of 210 N and actuation amplitude of 200 N.

First of all, even though the carbon fiber coil goes through the entire body of the bobbin, a significant strain is still noted. This may be due to bending in the carbon fiber tubes due to the compressive force. In order to determine the occurrence of viscoelasticity or the occurrence of other nonlinear losses, the displacement is plotted against the force for both the original plastic bobbin coil and the co-wound coil. The results are shown in Figure 28.

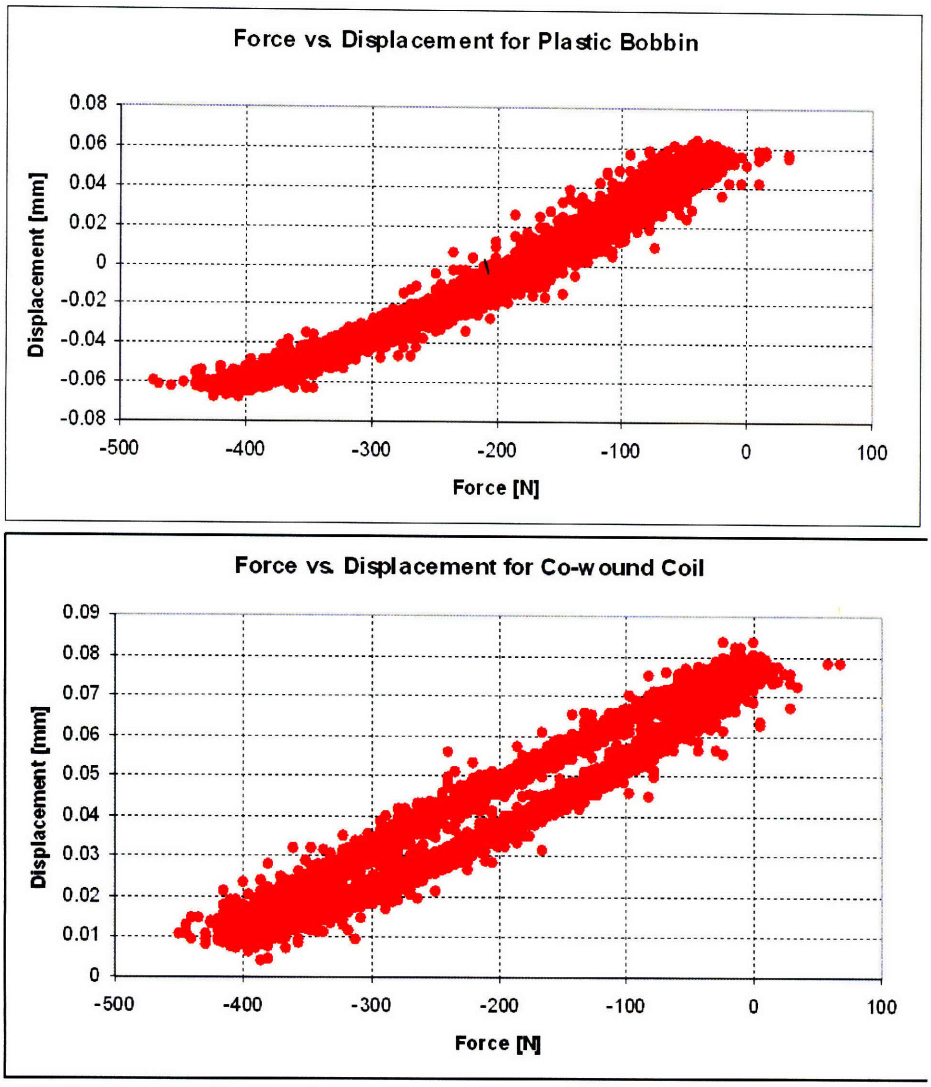

Figure 30: The displacement vs. force to show viscoelastic behavior and hysteresis. The polysulfone (top) shows viscoelasticity while the carbon fiber co-wound coil (bottom) shows hysteresis. Both coils are actuated at 200 N at 0.1 Hz.

The polysulfone shows interesting viscoelastic behavior because the displacement as a function of the force is slightly curved. However, it shows no hysteresis at this level of force. The carbon fiber and copper co-wound coil on the other hand, shows hysteresis. Carbon fiber is sometimes used as a damping material and with Figure 30 shows hysteresis at lower frequencies. As the compressive force increases, the displacement follows the top path and as the compressive force decreases, the displacement follows the bottom path. The displacement therefore lags the applied force and energy is stored into the co-winding. As the frequency is increased the hysteresis and the viscoelastic behavior begin to decrease and eventually disappear.

The stiffness of the material is the ratio of the force to the displacement. The stiffness constants were measured at many different frequencies and plotted in Figure 29.

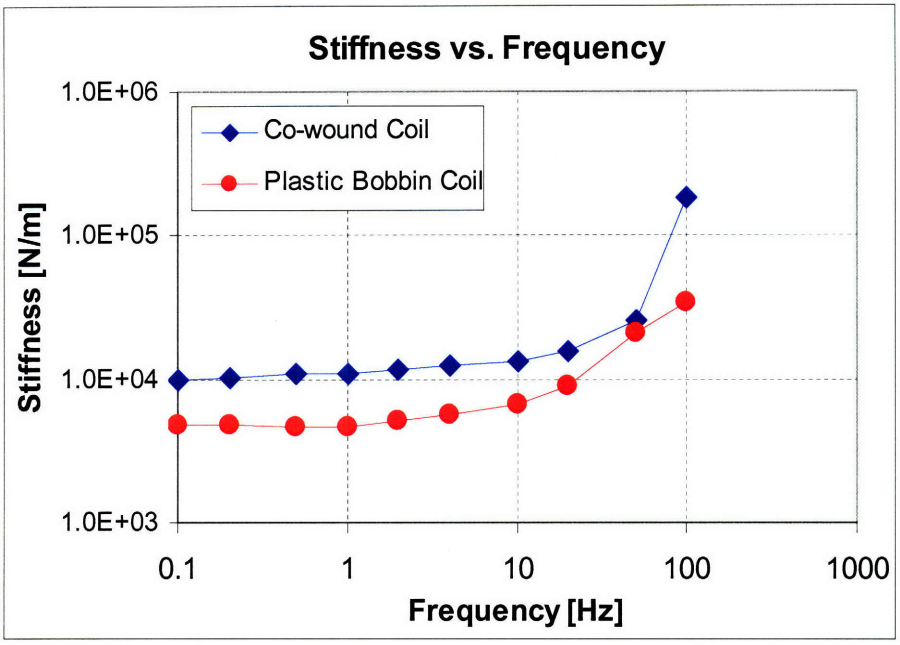

Figure 31: Plot of stiffness as a function of frequency for the plastic bobbin coil and the co-wound coil.

The stiffness for carbon fiber is on average 2.18 ± 0.13 times large as the stiffness of the original bobbin for frequencies up to 10 Hz and the stiffness of carbon fiber increases much faster because of its steeper slope at higher frequencies. Even though the average carbon fiber copper co-wound structure is lighter, it is also faster and stronger. One of the advantages of the carbon fiber, however, is its ability to maintain a higher stiffness for all frequencies.

5.4 Compression Strength

For higher force applications, an ultimate strength may be needed to understand the maximum possible loads a coil can undergo. The compressive strength of carbon fiber is lower than the tensile strength of carbon fiber. Therefore, compressive strength tests were conducted. Figure 30 shows an image of the typical crushed coil between the platens. There are many different failure modes discovered for the different materials. In the case of Figure 30, the original coil was a free-standing copper coil filled with resin and the final failure mode was when the alignment of the copper failed causes stresses on the resin. This then cause the resin to crack creating a series of popping sounds before the coil finally broke.

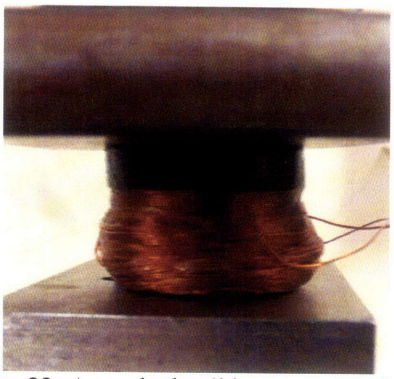

Figure 32: A crushed coil between the platens.

One failure mode observed for a free standing coil with resin was the cracking of the resin caused by instabilities in the copper windings. This caused free standing coils to fail on average at 5.54 kN. Figure 31 shows the failure modes of other types of coils.

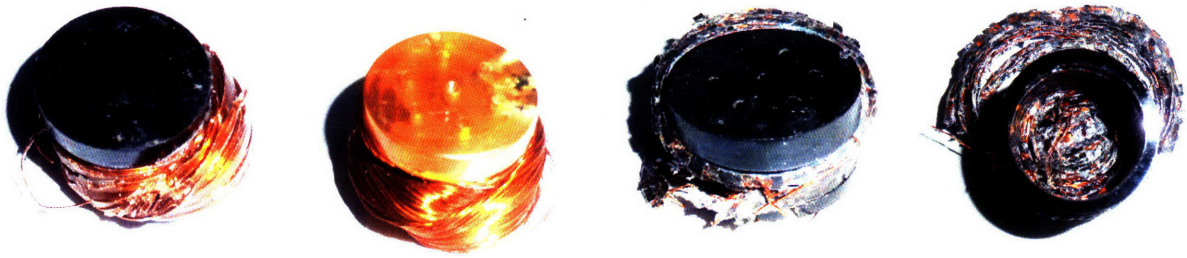

Figure 33: Crushed coils showing different failure modes. The coils from left to right are 1) a free-standing coil with laminating resin 2) a plastic bobbin coil 3) a co-wound coil from the top 4) a co-wound coil from the bottom exhibiting a different failure mode.

The plastic bobbin coils tended to fail at a slightly higher load where the bobbin would first develop a crack then putting loads onto the copper coil which subsequently collapsed. The average compressive force needed to break a plastic bobbin coil is 7.74 kN. Lastly carbon fiber co-wound coils tend to fail when set of five windings of coil displacing together in a group forcing a carbon fiber strand to break thereby increasing the load on one side of the coil. Then the entire coil would topple over. Another mode of failure is that the compressive stress causes entire sections of the rings to displace outwards as shown in the right most image in Figure 33. The inner and outer section of the coil would break and the entire section would displace outwards. The average compressive force needed for the co-wound coils to fail is 11.27 kN.

Figure 32 shows the force on the coil as a function of displacement. The polysulfone coils have smooth transition until about 1.2 mm where the displacement is no longer elastic but begins to

taper. Less force is needed at this point to displace the coil and it reaches its ultimate compressive strength. Then the coil begins to fail and the forces drop quickly as displacement increases rapidly.

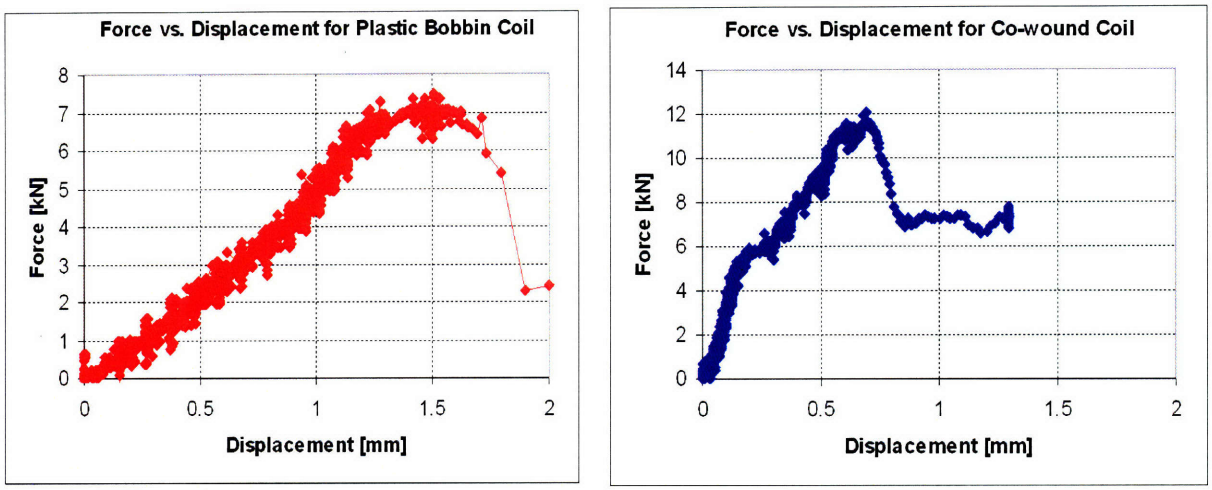

Figure 34: Force as a function of displacement for compressive strength testing for the plastic bobbin based coil (left) and the co-wound coil (right).

For the case of the co-wound coil, the force versus displacement function is more complex, up to approximately 6 kN, the coil shows linear elastic behavior, after 6 kN, the displacement is increases quickly without failing and the coil enters another elastic region. The transition from one region to another may be due to the fracture of some small segment in the coil that was bearing most of the load. However, at 6 kN, there were no visible signs of fracture. At approximately 11.7 kN, this particular coil failed quickly as the displacement rapidly increased.

6. Conclusions and Recommendations

Carbon fiber materials are strong and lightweight with many applications in industry. These and many other characteristics can become useful for use in voice coil technology. In particular, industries which use voice coils for high force and high frequency applications need stiff and strong materials. Carbon fiber and copper co-winding has many interesting properties that can help make innovations in the Lorentz force coils.

This paper proposes a method for manufacturing carbon fiber composite that is co-wound with a copper coil. The carbon tow is directed vertically to reduce eddy currents and to increase strength in the primary load bearing direction. In order to co-wind the material, a novel process for winding and curing had to be developed involving wet lay-up, compression molding and filament winding techniques. The co-winding process is shown to improve many aspects of Lorentz force coils.

The first aspect of improvement is the increased ability to move heat away from the copper coils. The improvement in the heat transfer is 15.7 % from simulations. The simulations also show that at higher temperatures, the co-wound takes a longer time to reach peak critical temperatures by an extra 0.21 to 0.26 seconds when exposed freely to the air. The co-winding process also improves the ability of the copper coils to transfer forces to the primary load bearing surface by constraining the coils laterally. At the same time, the lateral constraint prevents the coils from leaving their position and causing jamming inside a linear bearing.

Another improvement is the in the stiffness of the coil at lower loads. The co-wound coils were shown to be 2.18 ± 0.13 times stiffer than the original plastic bobbin for lower frequencies. This is an important finding for applications requiring high forces at lower speeds such as actuation for robotic fins. Lastly, the co-wound coils have a higher maximum compressive load of 11.27 kN which is much larger than the 7.74 kN that can be handled by plastic bobbins.

For future applications, an even faster method of producing the co-wound coils could be created involving full automation (with auto loading) and fast machine speeds. Clever geometries could

be used to achieve an automatic circular winding mechanism. Methods for injecting resin into carbon fiber at high pressures could also be explored which would allow a different type of high temperature resin with higher viscosities but faster curing times to be used. Pressure injection also has other benefits in that it forces out air bubbles more effectively than simple compression.

Carbon fiber and copper co-winding has many interesting benefits. Although it currently takes more time to manufacture than a bobbin, it is stronger, lighter, stiffer and better for transferring heat than the conventional plastic bobbin.

References

[1] Pioneer Electronics - 4-1, Meguro 1-Chome, Meguro-Ku, Tokyo 153-8654, Japan.

[2] Lockhart, M. Hypodermic Injector. U.S. Patent and Trademark Office. Patent 2,322,244. 22 June 1943.

[3] Ball, N.B. An Optimized Linear Lorentz-Force Actuator for Biorobotics and Needle-Free Injection. Thesis for Master of Science, MIT, 2007.

[4] Easton Sports, Inc., Bicycle Products Division, 7855 Haskell Avenue, Van Nuys, CA 91406-1999.

[5] Chung, D.D.L. Carbon Fiber Composites. Elsevier. 1994. http://www.knovel.com/knovel2/Toc.jsp?BookID=517&VerticalID=0.

[6] Askeland, D.R., *The Science and Engineering of Materials, 2d ed.* PWS-Kent, 1989.

[7] Ohsawa, T., Miwa, M., Kawade M. and Tsushima, E., J. Applied Polymer Science. 39(8), 1733-1743. 1990.

[8] Babu, M. S., Srikanth, G. and Biswas, S., "Composite Fabrication by Filament Winding - An Insight." http://www.tifac.org.in/news/acfil.htm.

[9] Composite Resources. 485 Lakeshore Parkway. Rock Hill, SC 29730.

[10] Boeing. 100 North Riverside, Chicago, Illinois, 60606-1596.

[11] Hercules Composite Structures, Hercules Inc.

[12] BEI Kimco Magnetics, 2470 Coral Street, Building "D", Vista, CA 92081-8430 USA.

[13] Taberner, A. J., Ball, N. B., Hogan, N.C. and Hunter, I.W. "A Portable Needle-free Jet Injector Based on a Custom High Power-density Voice-Coil Actuator." *Proceedings of the 28th IEEE EMBS Annual International Conference*. New York, 30 Aug 2006.

[14] Liu, D. Design and Characterization of a Compact Voice Coil for a Needle-Free Injection Device. Thesis for Bachelors of Science, MIT, 2006.

[15] Hogan, N. C., Hemond, B.D., Wendell, D.M., Taberner A. J., Hunter, I. W. "Delivery of Active Collagenase to Skin Using a Lorentz-Force Actuated Needle-Free Injector." *28th IEEE EMBS Annual International Conference*. 2006.

[16] CrossJect, 12, Quai Henri IV, 75004 PARIS, France.

[17] Kendall, M. A. F., Mitchell, T. J., Hardy M. P. and Bellhouse B.J. "The Ballistic Delivery of High Density, High-Velocity Micro-Particles into Excised Human Skin." *2001 Bioengineering Conference.* Vol. 50, 2001.

[18] Kendall, M. A. F., Wrighton Smith, P.W., and Bellhouse, B. J. "Transdermal Ballistic Delivery of Micro-Particles: Investigation into Skin Penetration." *World Congress on Medical Physics and Biomedical Engineering*. 2000.

[19] Bennet, S. Potter, C. "Pushing the Boundaries of Needle Free Injection," *Drug Delivery Report.* Glide Pharma. 2006. http://www.drugdeliveryreport.com/articles/ddr_aw06_article4.pdf.

[20] Quinlan, N.J., Kendall, M.A.F., Bellhouse, B.J., Ainsworth, R.W. "Investigations of gas and particle dynamics in first generation needle-free drug delivery devices," *Shock Waves*. 10, pg 395-404. 2001.

[21] Hemond, B.D. A Lorentz-force Actuated Controllable Needle-free Drug Delivery System. Thesis for Master of Science, MIT, 2006.

[22] Wendell, D. M. Controllable Needle-Free Injection Development and Verification of a Novel Device. Thesis for Master of Science, MIT, 2006.

[23] Hemond, B.D., Wendell, D. M., Hogan, N.D., Taberner, A. J., Hunter, I.W. "A Lorentz-Force Actuated Autoloading Needle-free Injector." *28th IEEE EMBS Annual International Conference*. 2006.

[24] MWS Wire Industries, 31200 Cedar Valley Drive, Westlake Village, CA 91362.

[25] Pro-Set Inc., 707 Martin St., P.O. Box 656, Bay City, MI 48707-0656.

[26] CST-The Composite Store 16330 Harris Road, Tehachapi, CA 93561.

[27] Aumann Berlin GmbH, Blomberger Weg 4, 13437 Berlin, Germany.

[28] Omega Engineering Inc., One Omega Drive, Stamford, CT 06907-0047

[29] Lienhard, J.H. IV, Lienhard J.H.V, *A Heat Transfer Textbook Third Edition*, Cambridge, Massachusetts: Phlogiston Press, 2003.

Appendix

Temperature Model – This code implements the temperature models for both the original plastic bobbin coil and the carbon fiber coils.

```
function TempModel(V, Rleads, Twinitial, tend, dt, inputfile, offset,
isbobbin)
%Written by Yi Chen 2008
%Undergraduate Thesis in Mechanical Engineering at MIT
%%%%%%%%%%%%%%%%%%%%%%%%%%%%%%%%%%%%%%%%%%%%%%%%%%%%%%%%%%%%%%%%%%%%%%%
%Bulk heat transfer determination
%%%%%%%%%%%%%%%%%%%%%%%%%%%%%%%%%%%%%%%%%%%%%%%%%%%%%%%%%%%%%%%%%%%%%%%

%Load Material and Geometric Constants
MatProperties;
GeoConstants;
data = inputfile;

%Other Constants
g = 9.806;
Tamb = 30;
beta = 1/Tamb;

%For bobbin wound coil
Area =d_wire^2/4*pi();
l1=pi()*(d_bobbin_middle+d_wire)*h_bobbin_coil/d_wire;
l2=pi()*(d_bobbin_middle+((3)^.5+1)*d_wire)*h_bobbin_coil/d_wire;
l3=pi()*(d_bobbin_middle+(2*(3)^.5+1)*d_wire)*h_bobbin_coil/d_wire;
l4=pi()*(d_bobbin_middle+(3*(3)^.5+1)*d_wire)*h_bobbin_coil/d_wire;
l5=pi()*(d_bobbin_middle+(4*(3)^.5+1)*d_wire)*h_bobbin_coil/d_wire;
l6=pi()*(d_bobbin_middle+(5*(3)^.5+1)*d_wire)*h_bobbin_coil/d_wire;
length = l1+l2+l3+l4+l5;
R = length*Copper_resist/Area;  %Resistance based on resistivity
Resistance = R+ Rleads;
C_mass = Area*length*Copper_den;
I = V/Resistance;
Pin = I*V;       %volumetric heat generation

%Changing Values
Tw1 = Twinitial;  %need to iterate on this value
Tw2 = Twinitial; %need to iteration on this value
qw1 = 0;    %initialize
qw2 = 0;     %initialize

count = 1;

for time = 0:dt:tend
    %Constants for Bobbin
    L = h_bobbin_coil;
    A1 = d_bobbin_outer*pi*h_bobbin_coil;
    A2 = d_bobbin_middle*pi*h_bobbin_coil;

    %Convection on outer wall
```

```
Tref1 = Tw1-0.83*(Tw1-Tamb);
k1 = AirProperties(Tref1, 'k');
alpha1 = AirProperties(Tref1, 'a');
mew1 = AirProperties(Tref1, 'v');
Pr1 = AirProperties(Tref1, 'pr');

Ra1 = g*beta*qw1*L^4/(k1*mew1*alpha1);
if (Ra1>10^9)
   Ra1 %Outputs if out of bounds
end
Nu1 = 0.73*Ra1^(1/3)/(1+(0.0492/Pr1)^(9/10))^(16/45);
h1 = Nu1*k1/L;
Rconv1 = 1/(h1*A1);

if isbobbin==1
    %Conduction on outer wall
    Rcond11 = (d_insul-d_insul_min)/2/(Enamel_ai_cond*A1);
    Rcond12 = (d_insul_min-d_copper)/2/(Enamel_p_cond*A1);
    Rcond1 = Rcond11+Rcond12;
else
    Rcond11 = (d_insul-d_insul_min)/2/(Enamel_ai_cond*A1);
    Rcond12 = (d_insul_min-d_copper)/2/(Enamel_p_cond*A1);
    Rcond13 = 1/4*d_wire/(Epoxy_cond*A1);
    Rcond14 = 96.5*10^(-6)/(CF_cond*1/2*A1);
    Rcond1 = Rcond11+Rcond12+Rcond13+Rcond14;
end

%Convection on inner wall
Tref2 = Tw2-0.83*(Tw2-Tamb);
k2 = AirProperties(Tref2, 'k');
alpha2 = AirProperties(Tref2, 'a');
mew2 = AirProperties(Tref2, 'v');
Pr2 = AirProperties(Tref2, 'pr');

Ra2 = g*beta*qw2*L^4/(k1*mew2*alpha2);
if (Ra2>10^9)
    Ra2 %Outputs if out of bounds
end
Nu2 = 0.73*Ra2^(1/3)/(1+(0.0492/Pr2)^(9/10))^(16/45);
h2 = Nu2*k1/L;
Rconv2 = 1/(h2*A2);

if isbobbin==1
    %Conduction on inner wall
    Rcond21 = (d_insul-d_insul_min)/2/(Enamel_ai_cond*A2);
    Rcond22 = (d_insul_min-d_copper)/2/(Enamel_p_cond*A2);
    Rcond23 = 1/4*d_wire/(AirProperties(Tw2,'k')*A2);
    Rcond24 = (t_bobbin)/(Bobbin_p_cond*A2);
    Rcond2 = Rcond21+Rcond22+Rcond23+Rcond24;
else
    Rcond21 = (d_insul-d_insul_min)/2/(Enamel_ai_cond*A2);
    Rcond22 = (d_insul_min-d_copper)/2/(Enamel_p_cond*A2);
    Rcond23 = 1/4*d_wire/(Epoxy_cond*A2);
    Rcond24 = 96.5*10^(-6)/(CF_cond*1/2*A2);
    Rcond2 = Rcond21+Rcond22+Rcond23+Rcond24;
end
```

```
    %Overall heat transer
    Uout = 1/(A1+A2)*(1/(Rconv1+Rcond1)+1/(Rconv2+Rcond2));

    %Transient Model
    Bi_outside = h1*t_bobbin_space/Copper_cond;
    Bi_inside = h2*t_bobbin_space/Copper_cond;

    if isbobbin ==1
        %Heat Capacity
        rho = Copper_den;
        V = length*pi*d_wire^2/4;
        cp = Copper_cp;
        rhop = Enamel_p_cond;
        Vp = length*pi*(d_insul^2/4-d_insul_min^2/4);
        cpp = Enamel_p_cp;
        rhoai = Enamel_ai_cond;
        Vai = length*pi*(d_insul_min^2/4-d_copper^2/4);
        cpai = Enamel_ai_cp;
        rhoair = AirProperties(Tw1, 'rho');
        Vair = h_bobbin_coil*pi*(d_bobbin_outer^2/4-d_bobbin_middle^2/4)-
length*pi*(d_wire^2/4);
        cpair = AirProperties(Tw1, 'cp');
        rhob = Bobbin_p_den;
        Vb=h_bobbin_coil*pi*(d_bobbin_middle^2/4-d_bobbin_inner^2/4);
        cpb=Bobbin_p_cp;
        En =
rho*V*cp+rhop*Vp*cpp+rhoai*Vai*cpai+rhoair*Vair*cpair+rhob*Vb*cpb;
    else
        rho = Copper_den;
        V = length*pi*d_wire^2/4;
        cp = Copper_cp;
        rhop = Enamel_p_cond;
        Vp = length*pi*(d_insul^2/4-d_insul_min^2/4);
        cpp = Enamel_p_cp;
        rhoai = Enamel_ai_cond;
        Vai = length*pi*(d_insul_min^2/4-d_copper^2/4);
        cpai = Enamel_ai_cp;
        rhor = Epoxy_den;
        Vr = h_bobbin_coil*pi*(d_bobbin_outer^2/4-d_bobbin_middle^2/4)-
length*pi*(d_wire^2/4);
        cpr = Epoxy_cp;
        rhocf = CF_den;
        Vcf=h_bobbin_coil*pi*(d_bobbin_middle^2/4-d_bobbin_inner^2/4);
        cpcf=Bobbin_p_cp;
        En = rho*V*cp+rhop*Vp*cpp+rhoai*Vai*cpai+rhor*Vr*cpr+rhocf*Vcf*cpcf;
    end


    %Temperature as a function of time
    c1 = (Uout*(A1+A2)/(En));
    c2 = Pin/(En)+(Uout*(A1+A2)/(En))*Tamb;
    Temperature(count) = c2/c1+(Twinitial-c2/c1)*exp(-c1*time);

    if isbobbin ==1;
```

```
        c1bobbin =
((1/(Rcond21+Rcond22+Rcond23))+(1/(Rconv2)))/(rhob*Vb*cpb);
        c2bobbin =
((1/(Rcond21+Rcond22+Rcond23))*Temperature(count)+(1/(Rconv2))*Tamb)/(rhob*Vb
*cpb);
        Tbobbin(count) = c2bobbin/c1bobbin+(Twinitial-
c2bobbin/c1bobbin)*exp(-c1bobbin*time);
        Tw1 = Temperature(count)-Rcond1/(Rconv1+Rcond1)*(Tamb-
Temperature(count));
        Tw2 = Tbobbin(count);
    else
        Tw1 = Temperature(count)-Rcond1/(Rconv1+Rcond1)*(Tamb-
Temperature(count));
        Tw2 = Temperature(count)-Rcond2/(Rconv2+Rcond2)*(Tamb-
Temperature(count));
    end

    %Saving Temperatures and qs
    Tw1track(count) = Tw1;
    Tw2track(count) = Tw2;
    qw1 = A1/(Rconv1+Rcond1)*(Temperature(count)-Tamb);
    qw2 = A2/(Rconv2+Rcond2)*(Temperature(count)-Tamb);
    Q1track(count) = 1/(Rconv1+Rcond1)*(Temperature(count)-Tamb);
    Q2track(count) = 1/(Rconv2+Rcond2)*(Temperature(count)-Tamb);

    count = count+1;
end

%Bobbin Temperature lag
Bi = 1/(Rconv2*A2)*t_bobbin/Bobbin_p_cond;
if isbobbin==1
    delay =
t_bobbin^2/((0.5063*2)^2*Bobbin_p_cond/(Bobbin_p_den*Bobbin_p_cp));
else
    delay = 0;
end

%Display
tend2 = tend+offset;
plot(offset:dt:tend2,Tw1track,offset+delay:dt:tend2+delay,Tw2track,
data(:,2),data(:,6),data(:,2),data(:,4) );
xlabel('Time(s)')
ylabel('Temperature(deg C)')
legend('Model of Outer Sensor in Free Air', 'Model of Inner Sensor in Free
Air', 'Outer Senor in Free Air', 'Inner Sensor in Free Air')
grid on;

plot(offset:dt:tend2,Q1track,offset:dt:tend2,Q2track)
xlabel('Time(s)')
ylabel('Heat Transfer (W/m^2K)')
legend('Outer Sensor Heat Transfer', 'Inner Sensor Heat Transfer')
grid on;
```

Stress Strain – This code is used to determine the stress strain properties of carbon fiber composites during the initial analysis

```
%Initialize Properties, Geometry, and Constants
MatProperties;
GeoConstants;

%Composite Modulus for CF based on orientation efficiency (in tension)
%Based on pg78 of Engineering Materials 1

Vf = 0:0.01:1;%volume fraction of fiber
Ef = CF_tmod;
Em = Epoxy_tmod;

Ecomp_h=Vf*Ef+(1-Vf)*Em;
Ecomp_l=1./(Vf/Ef+(1-Vf)/Em);

length = 49.1689;

Vepoxy = h_bobbin_coil*pi*(d_bobbin_outer^2/4-d_bobbin_middle^2/4)-
length*pi*(d_wire^2/4);
Vcarbon = h_bobbin_coil*pi*(d_bobbin_middle^2/4-d_bobbin_inner^2/4);
Vf_actual = Vcarbon/(Vepoxy+Vcarbon);
Ecomp_actual = Vf_actual*Ef+(1-Vf_actual)*Em;

plot(Vf,Ecomp_h,Vf,Ecomp_l,[Vf_actual Vf_actual Vf_actual], [0 Ecomp_actual
Ef]);
```

Geometric Constants – These constants are used to determine the geometry for different scripts

```
%Written by Yi Chen 2008
%Undergraduate Thesis in Mechanical Engineering at MIT
%%%%%%%%%%%%%%%%%%%%%%%%%%%%%%%%%%%%%%%%%%%%%%%%%%%%%%%%%%%%%%%%%%%%%%%%%%%
%Geometric Constants
%%%%%%%%%%%%%%%%%%%%%%%%%%%%%%%%%%%%%%%%%%%%%%%%%%%%%%%%%%%%%%%%%%%%%%%%%%%

%28 Gauge single build MW-35C wire properties
%Properties from MSW Wire Industries
d_copper_min=0.0125*0.0254;%0.0125inches
d_copper=0.0126*0.0254;%0.0126inches
d_copper_max=0.0127*0.0254;%0.0127inches
d_insul_min=0.0133*0.0254;%0.0133inches
d_insul=0.0137*0.0254;%0.0137inches
d_insul_max=0.0140*0.0254;%0.140inches

%Derived Quantities
d_wire = d_insul;

%Bobbin Dimensions (measured)
d_bobbin_outer=1.237*0.0254;%1.237inches
d_bobbin_inner=1.016*0.0254;%1.016inches
```

```
d_bobbin_middle=1.075*0.0254;%1.075inches
h_bobbin_coil = 1.486*0.0254;%1.486inches
h_bobbin_full = 1.852*0.0254;%1.852inches
h_bobbin_bottom = 0.0822*0.0254;%0.0822inches

%Derived Quantities
t_bobbin=(d_bobbin_middle-d_bobbin_inner)/2;
t_bobbin_space = (d_bobbin_outer-d_bobbin_middle)/2;
h_bobbin_top = h_bobbin_full-h_bobbin_coil-h_bobbin_bottom;
```

Material Properties – This code output the material properties

```
%Written by Yi Chen 2008
%Undergraduate Thesis in Mechanical Engineering at MIT
%%%%%%%%%%%%%%%%%%%%%%%%%%%%%%%%%%%%%%%%%%%%%%%%%%%%%%%%%%%%%%%%%%%%%%%%%%%
%Material Properties
%%%%%%%%%%%%%%%%%%%%%%%%%%%%%%%%%%%%%%%%%%%%%%%%%%%%%%%%%%%%%%%%%%%%%%%%%%%
%Conventions: The commented number is the one quoted from Matweb, the
%manufacturer or the supplier.  This number is the first one in the formula
%and it is converted into standard SI units

%Copper (inside copper coil)
Copper_den=8.96/1000*100^3; %8.96 g/cc
Copper_mod = 110*10^9;%110GPa
Copper_bmod = 140*10^9;%140GPa
Copper_poisson=0.35; %0.35
Copper_smod=46*10^9;%46 GPa
Copper_resist= 0.00000170/100;
Copper_cte=16.4*10^-6;%16.4 μm/m-°C
Copper_cp=0.385*1000;%0.385 J/g-°C
Copper_cond=385; %385 W/m-K
Copper_melt=1083.2;%1083.2 - 1083.6 °C
Copper_emiss=0.15; %0.15
Copper_reflec=0.63; %0.63

%polyester with A/I Topcoat (APT) or polyester with A/I Polyamideimide
(APTIG) (Class 200) (MW-35C) (JW-1177/14) (coil coating)
Enamel_temp = 200; %200C
Enamel_flow = 300; %300C
Enamel_friction = 0.02; % .02 to .06

%Polyester
Enamel_p_den=1.25/1000*100^3; %1.25 - 1.40 g/cc
Enamel_p_mod=2.70*10^9;%2.70 - 3.79 GPa
Enamel_p_dielectric=3.2;%3.2-5.7
Enamel_p_dstrength=12.2; %12.2 - 30.0 kV/mm
Enamel_p_cond=0.290;%0.290 W/m-K
Enamel_p_cp = 0.28*4.18400*1000;%0.28 cal/g/ C
Enamel_p_cte=100*10^-6;%100 - 207 μm/m-°C
Enamel_p_Tm=220;%220 - 255 °C

%Polyamide-imide
Enamel_ai_den=1.39/1000*100^3;%1.39 - 1.58 g/cc
Enamel_ai_strength=68.9*10^6;%68.9-124MPa
```

```
Enamel_ai_mod=2.41*10^9;%2.41 - 4.14 GPa
Enamel_ai_yeild=100*10^6;%27-207MPa
Enamel_ai_dielectric=3.9;%3.90 - 6.00
Enamel_ai_dstrength=18.7;%18.7 - 24.0 kV/mm
Enamel_ai_cte=25*10-6;%25.0 - 50.4 μm/m-°C
Enamel_ai_cond=0.259;%0.259 - 0.540 W/m-K
Enamel_ai_cp = 1470; %1470J/kg*K
Enamel_ai_Tg=275; %275C
Enamel_ai_deflecttemp=271; %271 - 286 °C

%Polysulfone (bobbin material)
Bobbin_p_den=1.22/1000*100^3;%1.22 - 1.60 g/cc
Bobbin_p_tultstrength= 6*10^6;%6.00 - 179 MPa
Bobbin_p_tstrength = 55.2*1^6;%55.2 - 160 MPa
Bobbin_p_elongation=1.5/100;%1.50 - 7.50%
Bobbin_p_mod = 10*10^9;%2.07 - 24.1 GPa
Bobbin_p_cyield=100*10^6;%13.0 - 176 MPa
Bobbin_p_cmod=2.0*10^9;%1.73 - 2.59 GPa
Bobbin_p_cof=0.28;%0.280 - 0.450
Bobbin_p_cte=56*10^-6;%56.0 - 103 μm/m-°C
Bobbin_p_cond=0.218;%0.218 - 0.600 W/m-K
Bobbin_p_deflection=200;%171 - 214 °C
Bobbin_p_Tg=266;%185 - 266 °C
Bobbin_p_cp = 1470; %1470J/kg*K

%Carbon Fiber (Standard Modulus)
CF_tension= 512*10^3*6894.75729;%512 ksi
CF_tmod= 33.4*10^6*6894.75729;%33.4 msi
CF_den= 1.76/1000*100^3;%1.76 g/cm^3
CF_elong=1.5/100;% 1.5%
CF_cond = 520;%W/mK
CF_cp = 2.69;%J/kg*K

%Proset Epoxy 125/229 at 15hr at RT 8hr at 82C
Epoxy_den= 9.3*119.826427;%9.3lb/gal
Epoxy_vis=450/1000; %450 cps        %Note 1 cP = 1 mPa·s
Epoxy_compression=14930*6894.75729; %14930psi
Epoxy_tension=9974*6894.75729;  %9974psi
Epoxy_elong= 4/100; %4%
Epoxy_tmod=4.22*10^5*6894.75729;%4.22*10^5psi
Epoxy_fstrength= 17515*6894.75729;%17515psi
Epoxy_fmod =5.15*10^5*6894.75729; %5.15*10^5psi
Epoxy_deflecttemp=(157-32)*5/9;%157F
Epoxy_Tg=(161-32)*5/9;%161F
Epoxy_ultimateTg=(172-32)*5/9;%172F
Epoxy_cond=0.23;%W/mK
Epoxy_cp = 1380;
```

Air Properties – This code outputs the air properties at different temperatures

```
function y=AirProperties(Temp,propertystring)
%Written by Yi Chen 2008
%Undergraduate Thesis in Mechanical Engineering at MIT
%%%%%%%%%%%%%%%%%%%%%%%%%%%%%%%%%%%%%%%%%%%%%%%%%%%%%%%%%%%%%%%%%%%%%%%%%%%%%%%
%Air Properties
```

```
%%%%%%%%%%%%%%%%%%%%%%%%%%%%%%%%%%%%%%%%%%%%%%%%%%%%%%%%%%%%%%%%%%%%%%%%%%%%

%Convert acceptable temperature to Celcius
Temp = Temp+273.15;

%Convert property string
switch propertystring
    case 'rho'
        property=2;
    case 'cp'
        property=3;
    case 'mew' %viscosity
        property=4;
    case 'v'
        property=5;
    case 'k' %conductivity
        property=6;
    case 'a'
        property=7;
    case 'pr'
        property=8;
end

%T rho cp mew v k a pr
airdata = [100 3.605 1039 0.711*10^(-5) 0.197*10^(-5) 0.00941 0.251*10^(-5)
0.784
150 2.368 1012 1.035*10^(-5) 0.437*10^(-5) 0.01406 0.587*10^(-5) 0.745
200 1.769 1007 1.333*10^(-5) 0.754*10^(-5) 0.01836 1.031*10^(-5) 0.731
250 1.412 1006 1.606*10^(-5) 1.137*10^(-5) 0.02241 1.578*10^(-5) 0.721
260 1.358 1006 1.649*10^(-5) 1.214*10^(-5) 0.02329 1.705*10^(-5) 0.712
270 1.308 1006 1.699*10^(-5) 1.299*10^(-5) 0.02400 1.824*10^(-5) 0.712
280 1.261 1006 1.747*10^(-5) 1.385*10^(-5) 0.02473 1.879*10^(-5) 0.711
290 1.217 1006 1.795*10^(-5) 1.475*10^(-5) 0.02544 2.078*10^(-5) 0.710
300 1.177 1007 1.857*10^(-5) 1.578*10^(-5) 0.02623 2.213*10^(-5) 0.713
310 1.139 1007 1.889*10^(-5) 1.659*10^(-5) 0.02684 2.340*10^(-5) 0.709
320 1.103 1008 1.935*10^(-5) 1.754*10^(-5) 0.02753 2.476*10^(-5) 0.708
330 1.070 1008 1.981*10^(-5) 1.851*10^(-5) 0.02821 2.616*10^(-5) 0.708
340 1.038 1009 2.025*10^(-5) 1.951*10^(-5) 0.02888 2.821*10^(-5) 0.707
350 1.008 1009 2.090*10^(-5) 2.073*10^(-5) 0.02984 2.931*10^(-5) 0.707
400 0.8821 1014 2.310*10^(-5) 2.619*10^(-5) 0.03328 3.721*10^(-5) 0.704
450 0.7840 1021 2.517*10^(-5) 3.210*10^(-5) 0.03656 4.567*10^(-5) 0.703
500 0.6414 1040 2.713*10^(-5) 3.845*10^(-5) 0.03971 5.464*10^(-5) 0.704
550 0.6414 1040 2.902*10^(-5) 4.524*10^(-5) 0.04277 6.412*10^(-5) 0.706
600 0.5880 1051 3.082*10^(-5) 5.242*10^(-5) 0.04573 7.400*10^(-5) 0.708];

count2 = 1;
while (airdata(count2,1)<Temp);
    count2 = count2+1;
    if airdata(count2,1) ==550;
        y = airdata(count2,property);
        Temp = 550;
    end

end

if airdata(count2,1) <600 && count2>1;
```

```
    maxproperty = airdata(count2,property);
    minproperty = airdata(count2-1, property);
    interval = airdata(count2,1)-airdata(count2-1,1);

    %interpolate for value
    y= (maxproperty-minproperty)/interval*(Temp-airdata(count2-
1,1))+minproperty;
elseif count2==1
    y = airdata(count2,property);
end
```